Bulletin of Mathematical Biology (2019) 81:2290–2322
https://doi.org/10.1007/s11538-019-00606-z

Society for Mathematical Biology

Metastability as a Coexistence Mechanism in a Model for Dryland Vegetation Patterns

Lukas Eigentler[1] · **Jonathan A. Sherratt**[1]

Received: 17 December 2018 / Accepted: 11 April 2019 / Published online: 22 April 2019

Abstract

Vegetation patterns are a ubiquitous feature of water-deprived ecosystems. Despite the competition for the same limiting resource, coexistence of several plant species is commonly observed. We propose a two-species reaction–diffusion model based on the single-species Klausmeier model, to analytically investigate the existence of states in which both species coexist. Ecologically, the study finds that coexistence is supported if there is a small difference in the plant species' average fitness, measured by the ratio of a species' capabilities to convert water into new biomass to its mortality rate. Mathematically, coexistence is not a stable solution of the system, but both spatially uniform and patterned coexistence states occur as metastable states. In this context, a metastable solution in which both species coexist corresponds to a long transient (exceeding 10^3 years in dimensional parameters) to a stable one-species state. This behaviour is characterised by the small size of a positive eigenvalue which has the same order of magnitude as the average fitness difference between the two species. Two mechanisms causing the occurrence of metastable solutions are established: a spatially uniform unstable equilibrium and a stable one-species pattern which is unstable to the introduction of a competitor. We further discuss effects of asymmetric interspecific competition (e.g. shading) on the metastability property.

Keywords Metastability · Vegetation patterns · Species coexistence · Pattern formation · Reaction–diffusion systems · Semi-arid landscapes

Lukas Eigentler was supported by The Maxwell Institute Graduate School in Analysis and its Applications, a Centre for Doctoral Training funded by the UK Engineering and Physical Sciences Research Council (Grant EP/L016508/01), the Scottish Funding Council, Heriot-Watt University and the University of Edinburgh.

✉ Lukas Eigentler
le8@hw.ac.uk

Jonathan A. Sherratt
J.A.Sherratt@hw.ac.uk

[1] Department of Mathematics, Maxwell Institute for Mathematical Sciences, Heriot-Watt University, Edinburgh EH14 4AS, UK

1 Introduction

Vegetation patterns in semi-arid climate zones are a prime example of a self-organising principle in ecology (Deblauwe et al. 2008; Valentin et al. 1999). One of the main mechanisms that creates such a mosaic of biomass and bare soil is a modification of soil properties by plants that induces a water redistribution feedback loop (Meron 2012, 2016, 2018; Rietkerk and van de Koppel 2008). On bare ground only small amounts of water are able to infiltrate into the soil and water run-off occurs, while in regions covered by biomass the soil's water infiltration capacity is increased. Dense plant patches therefore act as sinks and deplete soil water in regions of bare ground (Eldridge et al. 2000; Thompson et al. 2010). This redistribution of the limiting resource drives further growth in vegetation patches and thus closes the feedback loop.

Drylands account for approximately 41% of the Earth's land mass and are home to a similar proportion (38%) of the world's human population. The sizes of arid and semi-arid regions that suffer from land degradation are expected to increase over the coming decades due to climate change (Reynolds et al. 2007). Vegetation patterns are a characteristic feature of such fragile ecosystems. Patterns have been detected in semi-desert regions in the African Sahel (Deblauwe et al. 2012; Müller 2013; Thiery et al. 1995; White 1971; Worrall 1959), Somalia (Gowda et al. 2018; Hemming 1965), Australia (Dunkerley and Brown 2002; Heras et al. 2012; Tongway and Ludwig 1990), Israel (Buis et al. 2009; Sheffer et al. 2013) and Mexico and the US (Cornet et al. 1988; Deblauwe et al. 2012; Montana et al. 1990; Montana 1992; Pelletier et al. 2012; Penny et al. 2013). Changes to characteristic features of vegetation patterns in these regions such as the pattern wavelength, the area fraction covered by biomass or the recovery time from perturbations can act as early indicators of desertification as they provide a useful tool in predicting further changes to ecosystems (Corrado et al. 2014; Dakos et al. 2011; Gowda et al. 2016; Kéfi et al. 2007; Rietkerk et al. 2004; Saco et al. 2018; Zelnik et al. 2018). This is an issue of considerable socio-economic importance since agriculture is a major contributor to the economy in many drylands (United Nations Convention to Combat Desertification 2017). For example, in sub-Saharan Africa livestock frequently graze on spatially patterned vegetation. Thus, changes in vegetation levels have a major effect on the livestock sector, which makes a very significant contribution to GDP, e.g. 20% in Chad, 15% in Mali, 12% in Niger and 7.5% in Burkina Faso (Dickovick 2014; United Nations Food and Agriculture Organization 2005), with involvement of high proportions of the population [e.g. 40% in Chad (Dickovick 2014)].

Due to the temporal and spatial scales involved in the evolution of vegetation patterns, these ecosystems cannot be recreated in a laboratory setting. To gain a better understanding of the pattern dynamics, a number of mathematical models have been proposed (see Borgogno et al. 2009; Zelnik et al. 2013 for reviews). In particular, modelling efforts based on partial differential equations, most notably by Gilad et al. (2004, 2007a) and HilleRisLambers et al. (2001), Rietkerk et al. (2002), provide a rich framework for mathematical analysis. One model that stands out due to its simplicity is the Klausmeier model (Klausmeier 1999), which provides a deliberately basic description of the plant-water dynamics in semi-arid environments. The highly accessible nature of the model enables a detailed model analysis (e.g. by Bennett and

Sherratt 2018; Consolo et al. 2019; Eigentler and Sherratt 2018; Sherratt 2005, 2010, 2011, 2013b, c, d; Sherratt and Lord 2007; Siteur et al. 2014a; Ursino and Contarini 2006). Recent advances in remote sensing technology using satellite data provide a promising tool to test model predictions on pattern resilience (Bastiaansen et al. 2018; Gandhi et al. 2018).

Most models in this context only consider a single plant species or combine several species into one single variable. However, vegetation patches often consist of a mix of herbaceous and woody species, where the latter can usually be found in the centre of a patch, surrounded by the former (d'Herbès et al. 2001; Seghieri et al. 1997). Previous simulation-based studies of dryland ecosystem models have indeed been able to reproduce patterns in which two species coexist by considering a variety of different mechanisms and feedbacks that enable diversity in ecosystems (Baudena and Rietkerk 2013; Callegaro and Ursino 2018; Gilad et al. 2007b; Nathan et al. 2013; Ursino and Callegaro 2016). One such facilitative mechanism occurs in a system of two species in which only one plant type induces a pattern forming feedback. If, additionally, the non-pattern-forming species is superior in its water uptake and dispersal capabilities, then the pattern-forming species can act as an ecosystem engineer to facilitate coexistence of both species in patterned form (Baudena and Rietkerk 2013; Nathan et al. 2013). Even if patterns in which two species coexist are not observed as long-term solutions of a system, they can feature in a transition between two stable states. Gilad et al. (2007b) briefly report on the observation of coexistence patterns as a slow (several hundred years) transient during which patterns form due to facilitation between two species before eventually one of the species becomes extinct as competitive feedbacks take over. A different mechanism that enables coexistence of two species in both uniform and spatially patterned settings is adaptation to different ecological niches, such as soil moisture (Callegaro and Ursino 2018; Ursino and Contarini 2006).

In-phase spatial patterns are not the only phenomenon that is studied in the context of species coexistence. The existence of a multitude of localised patterns of one species in an otherwise uniform cover of a second species (homoclinic snaking) has also been observed as a possible form of coexistence in a mathematical model (Kyriazopoulos et al. 2014). The solution arises from a model that assumes a trade-off between root and shoot growth causing a balance between the competition for water and for light that supports coexistence. Other models are not able to make any statement on the coexistence of species, but yield valuable information on facilitation and competition between the plant types based on differences in traits such as their dispersal behaviour (Pueyo et al. 2010).

The savanna biome has also been studied by various non-spatial models that describe the dynamics of the relative abundances of grass, trees and water. While such models are unable to make any statements on the formation of spatial patterns, they still provide valuable insights into coexistence-preserving effects of processes such as precipitation intermittency (D'Onofrio et al. 2015), facilitation by grasses towards trees (Synodinos et al. 2015) or fire disturbances (Baudena et al. 2010; Scheiter et al. 2007).

Previous model analysis on species coexistence in semi-arid landscapes has mainly focussed on feedback loops induced through differences in the plant species' traits and their effects on multispecies plant communities. We are not aware of any studies that investigate effects of the differences in basic properties such as plant mortality or

plant growth rate on semi-arid vegetation patterns. In this paper, we aim to analytically address the question how the difference between two plant types can give rise to a multi-species metastable vegetation pattern [a unstable pattern whose instability is caused by a very small unstable eigenvalue (Potapov and Hillen 2005)] and how the pattern's properties are affected by changes to the difference between the species.

To do this, we introduce a multispecies model based on the Klausmeier model in Sect. 2. Numerical simulations of the model presented in Sect. 3 suggest two different origins of metastable coexistence patterns. These two pathways into the problem are closely examined through a linear stability analysis in Sects. 4 and 5. Finally, we discuss our results in Sect. 6.

2 Model

In this section, we lay out the framework used in this paper to analyse the coexistence of grass and trees in dryland ecosystems. We propose a model based on the extended Klausmeier model (Klausmeier 1999), which in dimensional form is

$$\frac{\partial u}{\partial t} = \overbrace{c_1 c_2 u^2 w}^{\text{plant growth}} - \overbrace{c_3 u}^{\substack{\text{plant}\\ \text{mortality}}} + \overbrace{c_4 \frac{\partial^2 u}{\partial x^2}}^{\text{plant dispersal}}, \tag{1a}$$

$$\frac{\partial w}{\partial t} = \underbrace{c_5}_{\text{rainfall}} - \underbrace{c_6 w}_{\text{evaporation}} - \underbrace{c_2 u^2 w}_{\substack{\text{water uptake}\\ \text{by plants}}} + \underbrace{c_7 \frac{\partial w}{\partial x}}_{\substack{\text{water}\\ \text{advection}}} + \underbrace{c_8 \frac{\partial^2 w}{\partial x^2}}_{\substack{\text{water}\\ \text{diffusion}}}, \tag{1b}$$

where $u(x,t)$ is the weight of plants per unit area and $w(x,t)$ is the mass of water per unit area in the one-dimensional space domain $x \in \mathbb{R}$ at time $t > 0$. The water supply (precipitation) of the system is assumed to be constant at rate c_5, while evaporation and plant loss effects are assumed to be proportional to the respective densities at rates c_6 and c_3, respectively. The nonlinearity in the terms describing water uptake and biomass growth arises due to a soil modification by plants. The term is the product of the density of the consumer u and of the available resource $c_2 u w$, which corresponds to water being able to infiltrate into the soil. The dependence on the plant density u in the latter term occurs due to a positive correlation between the plant density and the soil surface's permeability (Cornet et al. 1988; Rietkerk et al. 2000; Valentin et al. 1999). Plant growth is assumed to be proportional to water uptake (Rodriguez-Iturbe et al. 1999; Salvucci 2001), and water to biomass conversion takes place at rate c_1. In its original setting, the Klausmeier model is formulated to describe the dynamics on sloped terrain on which water flow downhill is modelled by advection at rate c_7. An extension includes diffusion of water at rate c_8 to account for water redistribution on flat ground and is well established now (e.g. Kealy and Wollkind 2012; Siteur et al. 2014a; van der Stelt et al. 2013; Zelnik et al. 2013). Plant dispersal is also modelled by a diffusion term (with diffusion rate c_4).

Both on flat ground and on sloped terrain, (1) captures the formation of patterns for sufficiently low levels of precipitation and their properties have been studied

extensively (Klausmeier 1999; Sherratt 2005; Sherratt and Lord 2007; Sherratt 2010, 2011, 2013b,c,d; Siteur et al. 2014a). In (1) the plant density u either describes one single species or accounts for the totality of all plant types in the ecosystem. While an ecosystem rarely consists of only one single species, estimation of species-dependent parameters such as the plant mortality rate c_3 may be impractical if u is comprised of many different species for which parameter estimates differ significantly [see, for example, estimates for tree and grass species by Klausmeier (1999)].

An extension of (1) that accounts for the differences between plant species in the same ecosystem can be obtained by separating the plant density u into $n \in \mathbb{N}$ different species u_i, $i = 1, \dots, n$ that satisfy (1) with an appropriate set of parameters in the absence of all other species. The model arising from this assumption is

$$\frac{\partial u_i}{\partial t} = \overbrace{k_1^{(i)} w u_i \left(\sum_{j=1}^{n} k_2^{(j)} u_j \right)}^{\text{plant growth}} - \overbrace{k_3^{(i)} u_i}^{\substack{\text{plant}\\ \text{mortality}}} + \overbrace{k_5^{(i)} \frac{\partial^2 u_i}{\partial x^2}}^{\text{plant dispersal}}, \tag{2a}$$

$$\frac{\partial w}{\partial t} = \underbrace{k_6}_{\text{rainfall}} - \underbrace{k_7 w}_{\text{evaporation}} - \underbrace{w \left(\sum_{j=1}^{n} u_j \right) \left(\sum_{j=1}^{n} k_2^{(j)} u_j \right)}_{\text{water uptake by plants}} + \underbrace{k_8 \frac{\partial w}{\partial x}}_{\substack{\text{water}\\ \text{advection}}} + \underbrace{k_9 \frac{\partial^2 w}{\partial x^2}}_{\substack{\text{water}\\ \text{diffusion}}}. \tag{2b}$$

for $i = 1, \dots, n$. In this multispecies model, the term describing water uptake by plants is, as in (1), the product of the water density w, the total plant density $\sum_{j=1}^{n} u_j$ and the soil's infiltration capacity $\sum_{j=1}^{n} k_2^{(j)} u_j$. The species-dependent constants $k_2^{(i)}$ account for the plant types' different contributions to the soil properties. The summands in $\sum_{j=1}^{n} u_j$ correspond to the consumption of water by each single species and are therefore not replicated in the term describing plant growth. Thus, the addition of new biomass of species u_i with water to biomass conversion rate $k_1^{(i)}$ only depends on the water density, the soil's infiltration capacity and the density of species u_i itself. The remaining assumptions are identical to those taken in the formulation of (1), i.e. $k_3^{(i)}$ and $k_5^{(i)}$ denote the mortality and diffusion rates of species u_i, respectively; k_6 is the constant amount of rainfall which adds water to the system; and k_7, k_8, and k_9 are the evaporation, advection and diffusion rates of water, respectively.

In (2) no direct interspecific interaction takes place. Instead plant species only compete indirectly through depletion of the limiting resource—water. Models of this type, in which species compete for the same limiting resource without any direct competition between the different types, do not provide a framework able to describe coexistence as the species that can tolerate the lowest level of the limiting resource outcompetes all competitors (Tilman 1982). Thus, a description of an ecosystem in which plant species coexist needs to take interspecific dynamics, such as shading, into account.

For simplicity we restrict the model to a system on flat ground of two plant species u_1 and u_2 only, in which one species inhibits the other by increasing its competitor's mortality rate but its own mortality rate remains unaffected by the presence of the other species. An alternative approach to model direct interspecific competition would be a reduction of a species' biomass growth rate (Kyriazopoulos et al. 2014). A classic example of such an one-sided inhibitory direct interaction is two species, such as a herbaceous and a woody species, where the latter grows much taller than the former and thus imposes a shading effect on its competitor. Shading may also have a facilitative effect on plants and induce a positive feedback loop due to a reduction in evaporation (Baudena and Rietkerk 2013; Gilad et al. 2007b). In contrast to a one-sided inhibitory shading effect, shading-induced evaporation reduction affects both species as beneficial effects occur indirectly through a variation in resource availability. Thus, the nonlinearity in the plant densities of the water consumption and plant growth terms can account for such a beneficial effect as it collectively describes all positive feedback loops increasing the growth of biomass.

Adding an inhibitory shading term to (2) with $n = 2$, we propose the model studied in this paper, which is

$$\frac{\partial u_1}{\partial t} = \overbrace{k_1^{(1)} w u_1 \left(k_2^{(1)} u_1 + k_2^{(2)} u_2\right)}^{\text{plant growth}} - \overbrace{k_3^{(1)} u_1}^{\text{plant mortality}} - \overbrace{k_4 u_1 u_2}^{\text{interspecific competition}} + \overbrace{k_5^{(1)} \frac{\partial^2 u_1}{\partial x^2}}^{\text{plant dispersal}}, \tag{3a}$$

$$\frac{\partial u_2}{\partial t} = \overbrace{k_1^{(2)} w u_2 \left(k_2^{(1)} u_1 + k_2^{(2)} u_2\right)}^{\text{plant growth}} - \overbrace{k_3^{(2)} u_2}^{\text{plant mortality}} + \overbrace{k_5^{(2)} \frac{\partial^2 u_2}{\partial x^2}}^{\text{plant dispersal}}, \tag{3b}$$

$$\frac{\partial w}{\partial t} = \underbrace{k_6}_{\text{rainfall}} - \underbrace{k_7 w}_{\text{evaporation}} - \underbrace{w\left(u_1 + u_2\right)\left(k_2^{(1)} u_1 + k_2^{(2)} u_2\right)}_{\text{water uptake by plants}} + \underbrace{k_9 \frac{\partial^2 w}{\partial x^2}}_{\text{water diffusion}}. \tag{3c}$$

The shading effect causes species u_2 to impose an additional mortality effect on u_1 that is dependent on the density u_2, while u_1 does not have such an effect on u_2. The results presented in this paper are robust to changes in the functional response of this shading effect. Results for shading effects with a Holling type II and Holling type III functional response show no qualitative difference to the algebraically simpler term in (3). Table 1 provides an overview of parameter estimates used in the model. As indicated in the table, we were able to obtain estimates for parameters from previous models on dryland vegetation, except for the rate of the direct interspecific interaction k_4. However, our model analysis in Sects. 4 and 5 suggests a suitable range for the shading parameter that yields biologically relevant results and we briefly discuss effects caused by deviations from this range.

A suitable nondimensionalisation for the model is

$$u_1 = \left(\frac{k_7}{k_2^{(1)}}\right)^{\frac{1}{2}} \widetilde{u}_1, \quad u_2 = \left(\frac{k_7}{k_2^{(1)}}\right)^{\frac{1}{2}} \widetilde{u}_2, \quad w = \frac{k_7^{\frac{1}{2}}}{k_1^{(1)}\left(k_2^{(1)}\right)^{\frac{1}{2}}}\widetilde{w},$$

$$x = \left(\frac{k_5^{(1)}}{k_7}\right)^{\frac{1}{2}} \widetilde{x}, \quad t = \frac{1}{k_7}\widetilde{t}.$$

The model thus becomes

$$\frac{\partial u_1}{\partial t} = w u_1 (u_1 + H u_2) - B_1 u_1 - S u_1 u_2 + \frac{\partial^2 u_1}{\partial x^2}, \tag{4a}$$

$$\frac{\partial u_2}{\partial t} = F w u_2 (u_1 + H u_2) - B_2 u_2 + D\frac{\partial^2 u_2}{\partial x^2}, \tag{4b}$$

$$\frac{\partial w}{\partial t} = A - w - w (u_1 + u_2)(u_1 + H u_2) + d\frac{\partial^2 w}{\partial x^2}, \tag{4c}$$

after dropping the $\widetilde{\cdot}$'s for brevity, where

$$A = \frac{k_1^{(1)}\left(k_2^{(1)}\right)^{\frac{1}{2}} k_6}{k_7^{\frac{3}{2}}}, \quad B_1 = \frac{k_3^{(1)}}{k_7}, \quad B_2 = \frac{k_3^{(2)}}{k_7}, \quad S = \frac{k_4}{\left(k_2^{(1)} k_7\right)^{\frac{1}{2}}},$$

$$F = \frac{k_1^{(2)}}{k_1^{(1)}}, \quad H = \frac{k_2^{(2)}}{k_2^{(1)}}, \quad D = \frac{k_5^{(2)}}{k_5^{(1)}}, \quad d = \frac{k_9}{k_5^{(1)}}.$$

The constants A and B_i are combinations of several of the original model's parameters, but represent rainfall and plant mortality, respectively. The ratios F, H and D describe the differences in the plant species' water to biomass conversion rates, the effects on the soil's infiltration capacity and the diffusion coefficients, respectively. Finally, d quantifies the ratio of the rate of water diffusion to that of the diffusion of plant species u_1. Table 1 includes estimates for the nondimensional parameters.

In the analysis of the model, we assume that u_1 is a herbaceous species and allow u_2 to vary between another grass species and a woody vegetation type. The parameters of u_1 are fixed throughout the analysis and act as a reference point. To investigate how the difference between two plant species affects the plant-water dynamics of the system, the parameters of u_2 are varied and comparisons to the fixed species u_1 are made. For brevity we refer to the two plant densities as grass and trees, even if u_2 differs only slightly from u_1. Parameter estimates (see Table 1) suggest that trees' rate of mortality is less than that of grasses ($B_2 < B_1$), trees convert water into biomass less efficiently ($F < 1$), trees affect the soil's water infiltration rate less severely per unit biomass ($H < 1$) and trees disperse at a slower rate than grass ($D < 1$). We further assume that the inhibitory effect of shading intensifies as the species difference increases.

Table 1 Overview of parameters in (3) and (4)

Parameter	Units	Estimates	Description
$k_1^{(1)}$	(kg biomass) (kg H_20)$^{-1}$	0.003 [1], 0.007 [2]	Water to biomass conversion rate for species u_1
$k_1^{(2)}$	(kg biomass) (kg H_20)$^{-1}$	0.002 [1], 0–0.01 [2]	Water to biomass conversion rate for species u_2
$k_2^{(1)}$	m^4 year^{-1} (kg biomass)$^{-2}$	100 [1]	Effect of plant species u_1 on water infiltration into the soil
$k_2^{(2)}$	m^4 year^{-1} (kg biomass)$^{-2}$	1.5 [1]	Effect of plant species u_2 on water infiltration into the soil
$k_3^{(1)}$	year^{-1}	1 [3], 1.8 [1]	Rate of plant loss for species u_1
$k_3^{(2)}$	year^{-1}	0.023 [3] 0.18 [1], 1.2 [4]	Rate of plant loss for species u_2
k_4	m^2 year^{-1} (kg biomass)$^{-1}$	—(see text)	Interspecific competition (shading)
$k_5^{(1)}$	m^2 year^{-1}	1 [1,5], 36.5 [2]	Rate of diffusion of u_1
$k_5^{(2)}$	m^2 year^{-1}	$6.25 \cdot 10^{-4}$ [4], 1 [1]	Rate of diffusion of u_2
k_6	(kg H_20) m^{-2} year^{-1}	250–750 [1], 0–1000 [4], 150–1200 [3], 0–365 [2]	Rainfall
k_7	year^{-1}	2 [2], 4 [1,4,5], 8 [3]	Rate of evaporation
k_9	m^2 year^{-1}	500 [5],	Rate of water diffusion

Parameter	Scaling	Estimates	Description
A	$k_1^{(1)}(k_2^{(1)})^{\frac{1}{2}} k_6 k_7^{-\frac{3}{2}}$	0.94–2.8 [1]	Nondimensionalised constant corresponding to rainfall
B_1	$k_3^{(1)} k_7^{-1}$	0.125 [3], 0.45 [1]	Nondimensionalised constant corresponding to the rate of plant loss of u_1
B_2	$k_3^{(2)} k_7^{-1}$	0.0029 [3], 0.045 [1]	Nondimensionalised constant corresponding to the rate of plant loss of u_2
F	$k_1^{(2)}(k_1^{(1)})^{-1}$	0–1 [2], 0.67 [1]	Ratio of plants' water to biomass conversion rates
H	$k_2^{(2)}(k_2^{(1)})^{-1}$	0.015 [1]	Ratio of plants' effects on water infiltration into soil
S	$k_4(k_2^{(1)} k_7)^{-\frac{1}{2}}$	—(see text)	Nondimensional constant corresponding to shading effect
D	$k_5^{(2)}(k_5^{(1)})^{-1}$	0–1 [1,2,4]	Ratio of plant species' diffusion rates
d	$k_9(k_5^{(1)})^{-1}$	500 [5]	Ratio of water and plant species u_1 diffusion rates

This table shows both the dimensional parameters in model (3) and the nondimensional parameters in (4), including their units (dimensional parameters) or scalings (nondimensional parameters), the estimated values that we use, and a brief description. The parameter estimates are obtained from [1]: Klausmeier (1999), [2]: Baudena and Rietkerk (2013), [3]: Synodinos et al. (2015), [4]: Gilad et al. (2007a) and [5]: Siteur et al. (2014a)

Thus, only this parameter region is analysed. In particular, to define a measure of species difference, we introduce a parameter $\chi \in [0, 1]$ that describes the extent to which the species differ. Thus, we set

$$\begin{aligned} B_2 &= B_1 - \chi(B_1 - b_2), \quad F = 1 - \chi(1 - f), \quad H = 1 - \chi(1 - h), \\ S &= s\chi, \quad D = 1 - \chi(1 - D_0), \end{aligned} \tag{5}$$

where B_1 is set to a typical mortality rate of a herbaceous species, b_2 to that of a woody species and f, h and D_0 to the smallest respective ratios between two differing species. If the species are the same (i.e. $\chi = 0$), then $B_2 = B_1$, $F = H = D = 1$ and $S = 0$. In this case, (4) simplifies to

$$\frac{\partial (u_1 + u_2)}{\partial t} = w (u_1 + u_2)^2 - B_1 (u_1 + u_2) + \frac{\partial^2 (u_1 + u_2)}{\partial x^2}, \tag{6a}$$

$$\frac{\partial w}{\partial t} = A - w - w (u_1 + u_2)^2 + d \frac{\partial^2 w}{\partial x^2}, \tag{6b}$$

by adding (4a) and (4b). This simplified model is the extended Klausmeier model (1) in nondimensional form on flat ground for plant density $u_1 + u_2$ and water density w.

3 Numerical Solutions of the Model

To motivate the analysis presented in Sects. 4 and 5, we present some typical solutions of (4) that are obtained by numerical integration. Despite the inclusion of direct interspecific competition in (4) and the associated existence of a pair of equilibria in which both species coexist (see Sect. 5), the system converges to a single-species state for any choice of parameters. The nature of this long-term behaviour depends on the parameter values used in the integration and may be a uniform or patterned state of either species. The transient to such an equilibrium state in which only one of the plant types is present may, however, occur as a very slow process (exceeding 10^3 years in dimensional parameters) in which both species coexist in either a patterned configuration or uniformly in space. Such a unstable state which nevertheless persists as a solution for a very long time (compared to the time taken to emerge from some initial configuration) is referred to as a metastable state in this context.

In the parameter setting (5) two distinct initial configurations from which such metastable states arise are established. If the initial condition is set to a state in which both plant species and the water density are uniform in space with a random perturbation added, then the solution remains in a metastable configuration in which both species coexist for a long time. If the rainfall is sufficiently low, the solution develops a patterned appearance in all three variables during the long transient. Eventually the metastable state reduces to a stable single-species equilibrium. The type of this equilibrium depends on the choice of parameters and, in particular, on the level of rainfall (see Fig. 1a). A sufficiently high level of rainfall leads to a spatially uniform solution, while lower amounts of precipitation cause convergence to a single-species pattern.

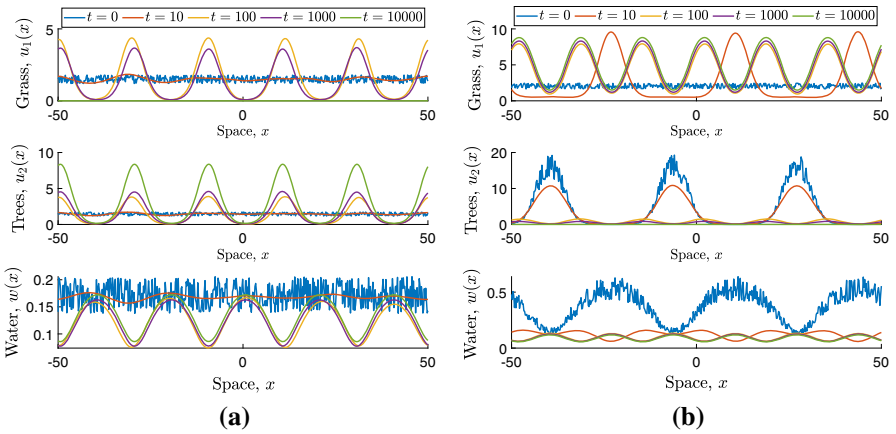

Fig. 1 Numerical solution of the multispecies model (4) showing metastable patterns of species coexistence. The simulations are performed by discretising the space domain into $M \in \mathbb{N}$ equidistant points, which yields a system of $3M$ ordinary differential equations. Periodic boundary conditions are imposed on the endpoints of the domain. The resulting system is integrated using the MATLAB ODE solver ode15s. In (**a**), $A = 1.5$ and $\chi = 0.2$ and the system is initially perturbed randomly from a state in which all densities are uniform in space. In (**b**) $A = 2.4$ and $\chi = 0.8$ and the simulation is started from a tree pattern to which a random perturbation is added. Both initial conditions are obtained from results of the one-species extended Klausmeier model (1). The other parameter values in all of the figures are $B_1 = 0.45$, $b_2 = 0.0055$, $f = 0.01$, $h = 0.01$, $s = 10^{-3}$, $d = 500$ and $M = 2^9$ (Color figure online)

The initial densities for the uniform state are chosen based on the steady states of the one-species Klausmeier model (1) (Klausmeier 1999).

A similar behaviour is exhibited by the model's solution if the initial condition of the system is set to a tree-only pattern that is obtained from the one-species Klausmeier model (1). To this configuration, a low density of the grass variable u_1 is added, as well as a random perturbation in all three variables. In this scenario, the grass density u_1 quickly adopts a pattern that is in phase with the tree density u_2. The solution remains in this configuration for a long time, but a sharp reduction in tree density and changes to the wavelength of the pattern may occur. Eventually a transition to a grass-only equilibrium occurs. As described above, the choice of this grass-only equilibrium to which the system eventually converges depends on the precipitation parameter A (see Fig. 1b).

Such metastable patterns are not only observed for the parameter values chosen in Fig. 1, but occur for a wide range of parameters. This motivates a closer investigation of the coexistence patterns and, in particular, their metastability. One possibility to gain a comprehensive understanding of the patterns' properties would be a systematic numerical investigation of the whole parameter space. Such an approach could involve the tracking of the time the system spends in the coexistence state under variations of both single parameters and combinations of multiple parameters, as well as a closer investigation of the pattern's properties such as its wavelength . However, the number of different parameters in the model poses a significant challenge for this approach. Instead, linear stability analysis can be used to study the existence and stability of such patterns, which is presented in Sects. 4 and 5.

4 Metastable Coexistence Patterns Arising from Stable One-Species Patterns

A common tool to study pattern formation in reaction–diffusion systems is linear stability analysis. Motivated by the simulation visualised in Fig. 1b, we use linear stability analysis to discuss the emergence of metastable patterns in which both species coexist from a stable one-species Turing-type pattern into which a new species is introduced.

Linear stability analysis is based on the growth/decay of perturbations to equilibria of the system. Depending on the choice of parameters (6) has up to seven spatially homogeneous steady states; a trivial state describing desert which is stable in the whole parameter space, and pairs of semi-trivial single-species steady states as well as a pair of equilibria that correspond to coexistence of both species. To differentiate between the two types of patterns addressed in this section, we strictly refer to a pattern to be of Turing type if it emerges from a steady state that is linearly stable to spatially uniform perturbations and becomes unstable upon introduction of spatial variation in the perturbation. An equilibrium of (6) is linearly stable to spatially homogeneous perturbations if all eigenvalues $\lambda_u \in \mathbb{C}$ of the system's Jacobian at the steady states satisfy $Re(\lambda_u) < 0$. For (4), the Jacobian is given by $J(u_1, u_2, w) = (j(u_1, u_2, w)_{k\ell})$, $k, \ell = 1, 2, 3$, where

$$\begin{aligned}
j\,(u_1, u_2, w)_{11} &= (Hw - S)\,u_2 + 2u_1 w - B_1,\\
j\,(u_1, u_2, w)_{12} &= u_1\,(Hw - S)\,,\\
j\,(u_1, u_2, w)_{13} &= u_1\,(u_1 + Hu_2)\,,\\
j\,(u_1, u_2, w)_{21} &= Fu_2 w,\\
j\,(u_1, u_2, w)_{22} &= 2Fw\left(\frac{u_1}{2} + Hu_2\right) - B_2,\\
j\,(u_1, u_2, w)_{23} &= Fu_2\,(u_1 + Hu_2)\,,\\
j\,(u_1, u_2, w)_{31} &= -w\,(2u_1 + (1 + H)\,u_2)\,,\\
j\,(u_1, u_2, w)_{32} &= -w\,((1 + H)\,u_1 + 2Hu_2)\,,\\
j\,(u_1, u_2, w)_{33} &= -u_1^2 - (1 + H)\,u_1 u_2 - Hu_2^2 - 1.
\end{aligned} \tag{7}$$

For an equilibrium that is linearly stable to spatially uniform perturbations, Turing-type patterns emerge if there exists a wavenumber $k > 0$ such that at least one eigenvalue $\lambda_s \in \mathbb{C}$ of $J - \mathrm{diag}(k^2, Dk^2, dk^2)$ has positive real part, i.e. $\max_{k\geq 0,\lambda_s}\{Re(\lambda_s)\} > 0$.

Although $\max_{k\geq 0,\lambda_s}\{Re(\lambda_s)\} > 0$ is a necessary condition for the development of a pattern from a spatial perturbation, $\max_{\lambda_u}\{Re(\lambda_u)\} < 0$ is not necessarily required. Spatial patterns also form if $0 < \max_{\lambda_u}\{Re(\lambda_u)\} \ll \max_{k\geq 0,\lambda_s}\{Re(\lambda_s)\}$. In this case a pattern (and the corresponding equilibrium) is unstable, but the difference in the growth rates gives rise to a transient pattern and the solution eventually tends to a stable state. In particular, if $\max_{\lambda_u}\{Re(\lambda_u)\} \ll 1$, this transient occurs at a slow rate as visualised in Fig. 1 and the pattern is metastable.

4.1 Turing-Type Patterns

Investigation of the existence of such metastable patterns requires a understanding of the model's single-species Turing-type patterns. Due to the nature of the model, the linear stability analysis of the single-species equilibria is almost identical to that of the extended Klausmeier model on flat ground, in which patterns emerge from a Turing bifurcation. The considerations for (4) only differ from those of the Klausmeier model through the existence of an additional condition that determines the stability to the introduction of the second species. Moreover, in case of the tree-only equilibria, the parameters F, H and D alter the stability conditions quantitatively.

For each plant species, there exists a pair of semi-trivial steady states in which only one plant species prevails. Provided $A > A^G_{\min} := 2B_1$, the grass equilibrium is

$$\left(\overline{u}_1^{G,\pm}, 0, \overline{w}^{G,\pm}\right) = \left(\frac{A \pm \sqrt{A^2 - 4B_1^2}}{2B_1}, 0, \frac{2B_1^2}{A \pm \sqrt{A^2 - 4B_1^2}}\right),$$

where the superscript G identifies it as a single-species grass state and $\pm$ indicates the choice of sign. Similarly, the pair of steady states describing a tree-only state is given by

$$\left(0, \overline{u}_2^{T,\pm}, \overline{w}^{T,\pm}\right) = \left(0, \frac{\xi_\pm}{2B_2H}, \frac{2B_2^2}{F\xi_\pm}\right),$$

provided the precipitation parameter exceeds $A^T_{\min,\mathrm{ex}} := 2B_2F^{-1}H^{-(1/2)}$, where $\xi_\pm = AFH \pm \sqrt{A^2F^2H^2 - 4B_2^2H}$.

4.1.1 Stability to Spatially Uniform Perturbations

The initial step in determining conditions for the existence of Turing-type patterns is linear stability analysis in a spatially uniform setting. Assuming no space dependence in (4), an equilibrium's stability is determined by the eigenvalues of the Jacobian with entries (7) evaluated at the equilibrium. For the grass-only steady state $(\overline{u}_1^{G,\pm}, 0, \overline{w}^{G,\pm})$, the Jacobian is

$$J^{G,\pm} = \begin{pmatrix} B_1 & \dfrac{2B_1^2H - SA - S\sqrt{A^2 - 4B_1^2}}{2B_1} & \dfrac{\left(A \pm \sqrt{A^2 - 4B_1^2}\right)^2}{4B_1^2} \\ 0 & B_1F - B_2 & 0 \\ -2B_1 & -B_1(1+H) & -\dfrac{A\left(A \pm \sqrt{A^2 - 4B_1^2}\right)}{2B_1^2} \end{pmatrix}.$$

Thus, the eigenvalues $\lambda_u^{G,\pm} \in \mathbb{C}$ satisfy

$$\left(B_1 F - B_2 - \lambda_u^{G,\pm}\right) \det \begin{pmatrix} B_1 - \lambda_u^{G,\pm} & \frac{\left(A \pm \sqrt{A^2 - 4B_1^2}\right)^2}{4B_1^2} \\ -2B_1 & -\frac{A\left(A \pm \sqrt{A^2 - 4B_1^2}\right)}{2B_1^2} - \lambda_u^{G,\pm} \end{pmatrix} = 0. \tag{8}$$

The eigenvalue $\lambda_{u,1}^{G,\pm} := B_1 F - B_2$ accounts for the introduction of the tree species u_2, while the remaining two eigenvalues are independent of any parameters associated with u_2. Indeed, the matrix in (8) is identical to that of the corresponding matrix obtained in the linear stability analysis of the Klausmeier model in which only a single species is considered. Thus, $(\overline{u}_1^{G,+}, 0, \overline{w}^{G,+})$ is linearly stable to spatially homogeneous perturbations if $A > A_{\min}^G$, $B_2 > B_1 F$ and $B_1 < 2$, while $(\overline{u}_1^{G,-}, 0, \overline{w}^{G,-})$ is linearly unstable for any choice of parameters (Klausmeier 1999; Sherratt 2005).

Similar to the analysis of the grass steady state, the tree equilibrium $(0, \overline{u}_2^{T,-}, \overline{w}^{T,-})$ is linearly unstable in the whole parameter space and $(0, \overline{u}_2^{T,+}, \overline{w}^{T,+})$ is linearly stable to spatially homogeneous perturbations if $A > A_{\min,\text{ex}}^T$, $B_2 < 2$ and

$$S > \frac{2B_2 H\,(B_2 - B_1 F)}{F\xi_+}. \tag{9}$$

Similar to the stability conditions of the single-species grass equilibrium, only criterion (9) accounts for the stability of $(0, \overline{u}_2^{T,+}, \overline{w}^{T,+})$ to the introduction of u_1. Thus, the stable (provided $A > A_{\min,\text{ex}}^T$ and $B_2 < 2$) single-species tree equilibrium becomes unstable to perturbations in the grass variable u_1 if the shading parameter is sufficiently small (see the difference between Fig. 2a, c). Rearranging (9) and combining it with the threshold $A_{\min,\text{ex}}^T$ for existence of the steady state yields that $(0, \overline{u}_2^{T,+}, \overline{w}^{T,+})$ exists and is linearly stable if $B_2 < 2$ and

$$A > A_{\min}^T := \begin{cases} \dfrac{2B_2}{F\sqrt{H}} & \text{if} \quad S > S_c \\ \dfrac{B_2\left(\left(B_1^2 H + S^2\right)F^2 - 2B_1 B_2 F H + B_2^2 H\right)}{(B_2 - B_1 F)\,F^2 H S} & \text{if} \quad S < S_c \end{cases}, \tag{10}$$

where $S_c := \sqrt{H}(B_2 - B_1 F)F^{-1}$. This lower bound is derived through calculation of the eigenvalues $\lambda_u^{T,\pm} \in \mathbb{C}$ of the Jacobian at $(0, \overline{u}_2^{T,\pm}, \overline{w}^{T,\pm})$ which satisfy

$$\left(\frac{2B_2 H\,(B_2 - B_1 F) - SF\xi_\pm}{2FHB_2} - \lambda_u^{T,\pm}\right) \det\left(J^{T,\pm} - \lambda_u^{T,\pm} I_2\right) = 0,$$

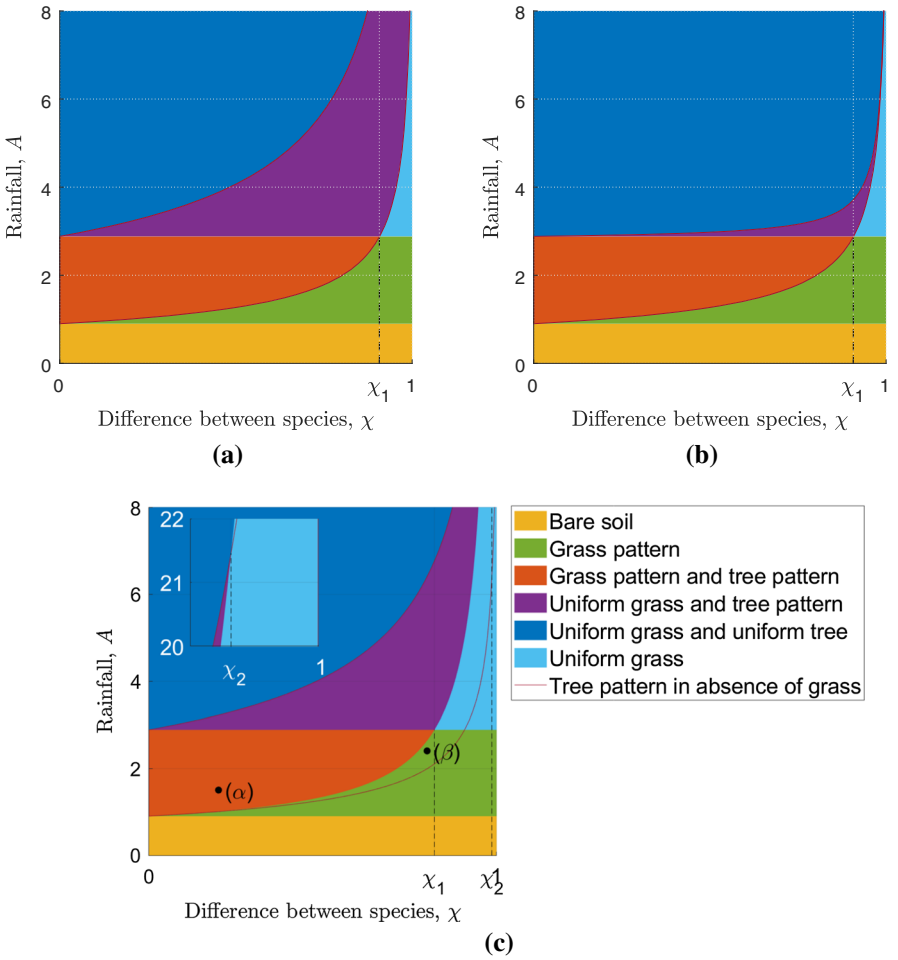

Fig. 2 Stability diagram for the semi-trivial steady states. The coloured areas combine the results of the linear stability analysis of the full model to spatially homogeneous perturbations and the respective one-species models in which spatially heterogeneous perturbations of the semi-trivial steady states lead to patterns in the parameter region (5). The solid line indicates the parameter region in which tree patterns form in the one-species model (12). The difference between (**a**) and (**c**) shows that this does not coincide with the corresponding parameter region in the multispecies model if S is small. The desert steady state is stable in the whole parameter plane. The area indicated in the figure only shows the region in which it is the only stable state. In (**a**) $s = 1$ and $D = 1 - \chi(1 - 0.01)$, which gives $S < S_c$ for all $0 < \chi < 1$; in (**b**) $s = 1$ and $D = 1$; and in (c) $s = 10^{-3}$ and $D = 1 - \chi(1 - 0.01)$. The inset in (**c**) shows the behaviour around $\chi = \chi_2$. The other parameter values in all of the figures are $B_1 = 0.45$, $b_2 = 0.0055$, $f = 0.01$, $h = 0.01$ and $d = 500$. The markers (α) and (β) refer to the parameter values used in the simulations presented in Fig. 1 (Color figure online)

where

$$J^{T,\pm} = \begin{pmatrix} B_2 & \dfrac{F\xi_\pm^2}{4B_2^2 H} \\ -\dfrac{2B_2}{F} & -\dfrac{AF\xi_\pm}{2B_2^2} \end{pmatrix},$$

and I is the identity matrix. Imposing a negativity condition on the root $\lambda_u^{C,+}$ given by the first factor of this product yields (9), while the remaining two eigenvalues are both negative if and only if $\mathrm{tr}(J^{T,\pm}) < 0$ and $\det(J^{T,\pm}) > 0$. For $(0, \overline{u}_2^{T,-}, \overline{w}^{T,-})$, $\det(J^{T,-}) < 0$ for any choice of parameters yielding its instability, while for $(0, \overline{u}_2^{T,+}, \overline{w}^{T,+})$, $\det(J^{T,+}) > 0$. Finally, stability requires $\mathrm{tr}(J^{T,+}) > 0$ which holds for all $B_2 < 2$.

Bistability of the tree-only steady state and the grass-only steady state requires stability of both semi-trivial equilibria to the introduction of the other species. Stability of the single-species grass equilibrium $(\overline{u}_1^{G,+}, 0, \overline{w}^{G,+})$ to the introduction of the tree species u_2, i.e. $B_2 > B_1 F$, occurs if the grass species has a superior water to biomass conversion to mortality rate, which we define to be a measure of a species' average fitness. To balance this disadvantage, stability of the tree-only state $(0, \overline{u}_2^{T,+}, \overline{w}^{T,+})$ to the introduction of the grass species u_1 necessitates the shading effect to be sufficiently large. Indeed, if $B_2 > B_1 F$ and $S < S_c$, then

$$A_{\min}^T = \frac{B_2\left(\left(B_1^2 H + S^2\right)F^2 - 2B_1 B_2 F H + B_2^2 H\right)}{\left(B_2 - B_1 F\right)F^2 H S},$$

which is decreasing in S below the threshold S_c. Thus, in the parameter region in which the grass-only steady state is stable, a decrease in the inhibitory shading effect of trees on grass increases the precipitation requirement for bistability of the tree-only and grass-only steady state. This is visualised in Fig. 2a, c. The threshold S_c defined in (10), which is of the same order of magnitude as the average fitness difference $B_2 - B_1 F$ between the species, describes the intensity of shading above which the tree equilibrium $(0, \overline{u}_2^{T,+}, \overline{w}^{T,+})$ is stable to the introduction of the grass species u_1 for any precipitation levels that guarantee the existence of the steady state. In other words, if the shading effect of u_2 on u_1 is sufficiently large, then $(0, \overline{u}_2^{T,+}, \overline{w}^{T,+})$ is always linearly stable to the introduction of the grass species u_1.

The bounds on the plant mortality parameters in the derivations above are sufficient but not necessary. However, parameter estimates consistently indicate that $B_1 < 2$ and $B_2 < 2$ (Klausmeier 1999; Synodinos et al. 2015) and thus we restrict the analysis to this region.

4.1.2 Conditions for the Formation of Turing-Type Patterns

Having established stability conditions for the single-species equilibria in a spatially uniform setting, we turn to spatially non-uniform perturbations of the steady states to determine the loci of Turing bifurcations. Typically, linear stability analysis is used

to study pattern formation by introducing perturbations of the steady state that are proportional to $\exp(\lambda_s t + ikx)$ for a growth rate $\lambda_s \in \mathbb{C}$ and wavenumber $k > 0$. Imposing such perturbations on the semi-trivial steady states, i.e. $(\overline{u}_1^{G,+}, 0, \overline{w}^{G,+})$ and $(0, \overline{u}_2^{T,+}, \overline{w}^{T,+})$, however, would yield negative plant densities, a biologically unrealistic scenario. To avoid this, the density of the species that vanishes at the steady state is kept at zero. This reduces the model to the one-species Klausmeier model with water diffusion (up to the constants F, H and D in case of $(0, \overline{u}_2^{T,+}, \overline{w}^{T,+})$), for which patterns form due to a diffusion-driven instability.

More precisely, for $(\overline{u}_1^{G,+}, 0, \overline{w}^{G,+})$ (4) reduces to

$$\begin{aligned}\frac{\partial u_1}{\partial t} &= w u_1^2 - B_1 u_1 + \frac{\partial^2 u_1}{\partial x^2},\\ \frac{\partial w}{\partial t} &= A - w - w u_1^2 + d\frac{\partial^2 w}{\partial x^2},\end{aligned}$$

which is the extended Klausmeier model on flat ground. The typical linear stability analysis approach outlined above yields that a pattern-forming instability occurs for

$$\begin{aligned}A_{\min}^{G} < A < A_{\max}^{G,+}&\\ := \frac{B_1^{\frac{3}{2}} d^{\frac{1}{2}} \left(3B_1^2 d^2 + 7B_1 d - 8 - 2\sqrt{2B_1^4 d^4 + 6B_1^3 d^3 - 8B_1 d}\right)^{\frac{1}{2}}}{dB_1 + 1},&\end{aligned} \tag{11}$$

provided $d > B_1^{-1}$. If $d < B_1^{-1}$, then $A_{\max}^{G,+} \in \mathbb{C}$ and no Turing bifurcation occurs.

Similarly, setting $u_1 = 0$ in (4), i.e. considering the tree-only steady state $(0, \overline{u}_2^{T,+}, \overline{w}^{T,+})$, yields

$$\frac{\partial u_2}{\partial t} = FHw u_2^2 - B_2 u_2 + D\frac{\partial^2 u_2}{\partial x^2}, \tag{12a}$$

$$\frac{\partial w}{\partial t} = A - w - Hw u_2^2 + d\frac{\partial^2 w}{\partial x^2}. \tag{12b}$$

Considerations identical to those in the analysis of the extended Klausmeier model show that an instability leading to the formation of a tree pattern occurs if

$$\begin{aligned}A_{\min,\mathrm{ex}}^{T} < A < A_{\max}^{T,+}&\\ := \frac{B_2^{\frac{3}{2}} d^{\frac{1}{2}} \left(3B_2^2 d^2 + 7DB_2 d - 8D^2 - 2\sqrt{2B_2^4 d^4 + 6DB_2^3 d^3 - 8D^3 B_2 d}\right)^{\frac{1}{2}}}{D^{\frac{1}{2}} F H^{\frac{1}{2}} (dB_2 + D)},&\end{aligned} \tag{13}$$

provided $d > DB_2^{-1}$. If $d < DB_2^{-1}$, then $A_{\max}^{T,+} \in \mathbb{C}$ and no Turing bifurcation occurs.

Condition (13) is equivalent to the ratio d/D of the diffusion coefficients exceeding a critical threshold. Thus, a lower rate of diffusion of the woody species increases the size of the parameter region supporting pattern formation. This phenomenon is visualised in the stability diagrams 2a, b. It is important to emphasise that the bifurcation point $A_{\max}^{T,+}$ is obtained by considering perturbations in u_2 and w only. The calculation of $A_{\max}^{T,+}$ does not take into account a possible introduction of the grass species u_1. Indeed, as the difference between Fig. 2a, c visualises, if the shading parameter S is sufficiently small, then there exists a parameter region in which a single-species tree pattern is stable only in the context of a single-species model. The instability to an introduction of the grass species u_1 occurs due to an increase in $A_{\min}^{T}$, given by (10), for decreasing S. For sufficiently small S, this causes $A_{\min}^{T} > A_{\min,\text{ex}}^{T}$ and thus a tree-only pattern cannot form for $A_{\min,\text{ex}}^{T} < A < A_{\min}^{T}$ if the assumption of $u_1 = 0$ is relaxed. Similarly, the pattern-forming condition (11) obtained for $(\overline{u}_1^{G,+}, 0, \overline{w}^{G,+})$ only applies if the steady state is stable to perturbations in u_2, i.e. if $B_2 > B_1 F$. In the stability diagrams in Fig. 2 a state is only assumed to occur if the introduction of the second species does not cause destabilisation. Even though this restricts the bistability region of both single-species equilibria, the numerical simulations presented in Sect. 3 suggest that this restriction does not apply to metastable patterns in which both species coexist. In particular, the simulation visualised in Fig. 1b, which corresponds to the (β) marker in Fig. 2c, lies outside the bistability region. Indeed, the parameter region $A_{\min,\text{ex}}^{T} < A < A_{\min}^{T}$, i.e. the region in which the tree pattern is stable in the one-species model but unstable to the introduction to the grass species, gives rise to a metastable pattern such as that shown in Fig. 1b and is closely examined in Sect. 4.2.

To address the effects caused by the difference between two plant species, we put particular emphasis on the parameter region given by (5), where the difference is described by a single parameter $0 < \chi < 1$ for simplicity. To focus on the possible coexistence of both plant types, we further restrict the parameter region to that of the grass-only steady state's stability, i.e. $A > 2B_1$ and $B_2 > FB_1$. The latter condition holds for all $0 < \chi < 1$ if $b_2 > fB_1$. The lowest levels of precipitation beyond the threshold $A = 2B_1$ that separates the parameter region in which only the trivial desert equilibrium is stable from bistability or tristability regions of plant states and the bare soil state, only support grass patterns. For a sufficiently small difference $\chi < \chi_1$ between the grass and tree species, an increase in rainfall along the precipitation gradient leads to a region in which the two patterned states are stable, before the uniform grass-only steady state gains stability and eventually also the uniform tree equilibrium becomes stable to form a parameter region in which there is bistability of both uniform steady states. If the difference between the species is larger than the threshold χ_1, then no bistability of both patterned states is possible. Instead, the uniform grass steady state becomes stable at rainfall levels that are lower than those required for a tree pattern to form (Fig. 2a–c). Finally, if $\chi > \chi_2 > \chi_1$, where the threshold χ_2 may be larger than unity, the system does not support the formation of tree patterns and there is a direct transition from the parameter region that supports only the uniform grass equilibrium to the region in which bistability of both uniform steady states occurs (Fig. 2c).

4.2 Metastable Patterns

The results of the preceding linear stability analysis not only show the existence of single-species Turing patterns, but in the parameter region $A^T_{\min,\mathrm{ex}} < A < A^T_{\min}$ also that of metastable patterns, such as the pattern visualised in Fig. 1b, in which both species coexist.

Provided it exists ($A > A^T_{\min,\mathrm{ex}}$), the tree-only equilibrium $(0, \overline{u}_2^{T,+}, \overline{w}^{T,+})$ is stable to spatially uniform perturbations in the tree density u_2 and the water density w for all biologically relevant parameter values and tree patterns emerge from the steady state due to a Turing-type instability for sufficiently low precipitation levels. An additional stability condition (9) arises from the introduction of the grass species u_1. If $(0, \overline{u}_2^{T,+}, \overline{w}^{T,+})$ is unstable to the introduction of u_1 ($A < A^T_{\min}$), the eigenvalue $\lambda^{T,+}_{u,1}$ corresponding to spatially uniform perturbations is of small size and thus gives rise to a metastable solution as shown in Fig. 1b. If in addition $Re(\lambda^{G,+}_{s,1}(k)) \gg \lambda^{T,+}_{u,1}$, where $\lambda^{T,+}_{s,1}(k) \in \mathbb{C}$ is the growth rate corresponding to a spatial perturbation with mode $k > 0$, the grass species quickly (compared to the time it takes to reach the stable grass-only state) adopts a patterned appearance in phase with the tree pattern during this transition. Indeed,

$$\lambda^{T,+}_{u,1} = \frac{2B_2H\,(B_2 - B_1F)}{F\left(AFH + \sqrt{A^2F^2H^2 - 4B_2^2F^2H}\right)} - S \leq \frac{2B_2}{AF^2}\,(B_2 - B_1F) \ll 1, \tag{14}$$

because tree mortality B_2 is of small size (see Table 1). Further, the condition $Re(\lambda^{G,+}_{s,1}(k)) \gg \lambda^{T,+}_{u,1}$ is satisfied unless parameter values are close to the grass-only steady state's Turing bifurcation locus. Thus, if a grass population is introduced into a stable tree pattern and causes destabilisation of this pattern as shown in Fig. 1b, the small size of the eigenvalue (if positive) yields a slow transition to the stable grass-only state. The difference $B_2 - B_1F$ plays a crucial role in the metastability property as it is the cause of the pattern's slow rate of destabilisation. Ecologically the small size of this difference corresponds to similar average fitness of both species. It is this balance that enables the coexistence of both species. The significance of $B_2 - B_1F$ is not a special feature of this particular case but also causes the metastability of patterns originating from spatially uniform initial conditions such as that used in the simulation visualised in Fig. 1a. This is discussed in more detail in Sect. 5.

Similar considerations suggest the possibility of metastable coexistence patterns that arise from the introduction of the tree species into a stable grass pattern that consequently becomes unstable. In this situation, however, the eigenvalue $\lambda^{G,+}_{u,1} = B_1F - B_2$ that corresponds to the introduction of the tree species is not necessarily small. Unless $\lambda^{G,+}_{u,1} \ll 1$, a perturbation of a grass pattern through the introduction of trees yields a quick transition to a tree pattern as a positive but not small value of $B_1F - B_2$ corresponds to a larger average fitness of the tree species.

4.2.1 Wavelength

A key feature of any regular pattern is its wavelength. While an extensive study of pattern wavelength requires tools from nonlinear analysis, linear stability analysis provides an insight into the wavelength of the patterns close to the bifurcation locus. Then, the pattern wavelength is typically determined by the wavenumber that corresponds to the largest growth rate. Given such a wavenumber $k_{\max}$ calculated in the derivation of the Turing bifurcation points, the corresponding pattern has wavelength $L = 2\pi/k_{\max}$.

From the preceding linear stability analysis, we find that the wavelength of the tree species is increasing with the parameter χ. Thus, for a constant level of precipitation, the more tree-like a species is, the longer is its pattern wavelength (Fig. 3c). Such a comparison requires bistability of both patterned states, which is not necessarily the case for all $0 \leq \chi \leq 1$, as indicated in Fig. 3. The wavelength of both species further increases with decreasing rainfall, which is in agreement with results for the Klausmeier model on sloped terrain (Sherratt 2005, 2013c).

The most unstable wavenumber is not necessarily the mode that is selected in a pattern. Hysteresis is known to occur in the single-species Klausmeier model (Sherratt 2013a; Siteur et al. 2014a) and may cause the selected mode to differ from the most unstable mode. It is thus informative to obtain bounds on the wavelength from linear stability analysis. These bounds show that both an increase in species difference and lower precipitation increase the range of possible wavelengths (Fig. 3a, b).

5 Metastable Coexistence Patterns Originate from a Coexistence Equilibrium

The analysis in Sect. 4 only explains patterns in which both species coexist in the parameter region $A^T_{\min,\mathrm{ex}} < A < A^T_{\min}$. The simulations presented in Sect. 3, however, suggest that metastable coexistence patterns occur in a wider range of the precipitation parameter A. In this section we show that Turing-type patterns of the tree species u_2 are not the only origin of metastable patterns. Additionally, metastable patterns of species coexistence can arise from an equilibrium in which both species coexist, which is the subject of this section.

Besides the trivial and semi-trivial equilibria discussed in Sect. 4, (4) also admits a pair of coexistence steady states $(\overline{u}_1^{C,\pm}, \overline{u}_2^C, \overline{w}^{C,\pm})$, where similar to the notation used for the single-species states the superscript C identifies the equilibrium as a coexistence state. The equilibria satisfy

$$\overline{u}_1^{C,\pm} = \frac{1}{2B_2}\left(AF - B_2(1+F)\,\overline{u}_2^C \right.$$
$$\left. \pm\sqrt{\left(AF + B_2(1+F)\,\overline{u}_2^C\right)^2 - 4B_2\left(-AFH\overline{u}_2^C + B_2\left(1+H\left(\overline{u}_2^C\right)^2\right)\right)}\right),$$
$$\overline{u}_2^C = \frac{B_2 - FB_1}{SF}, \quad \overline{w}^{C,\pm} = A - \frac{B_2}{F}\left(\overline{u}_1^{C,\pm} + \overline{u}_2^C\right),$$

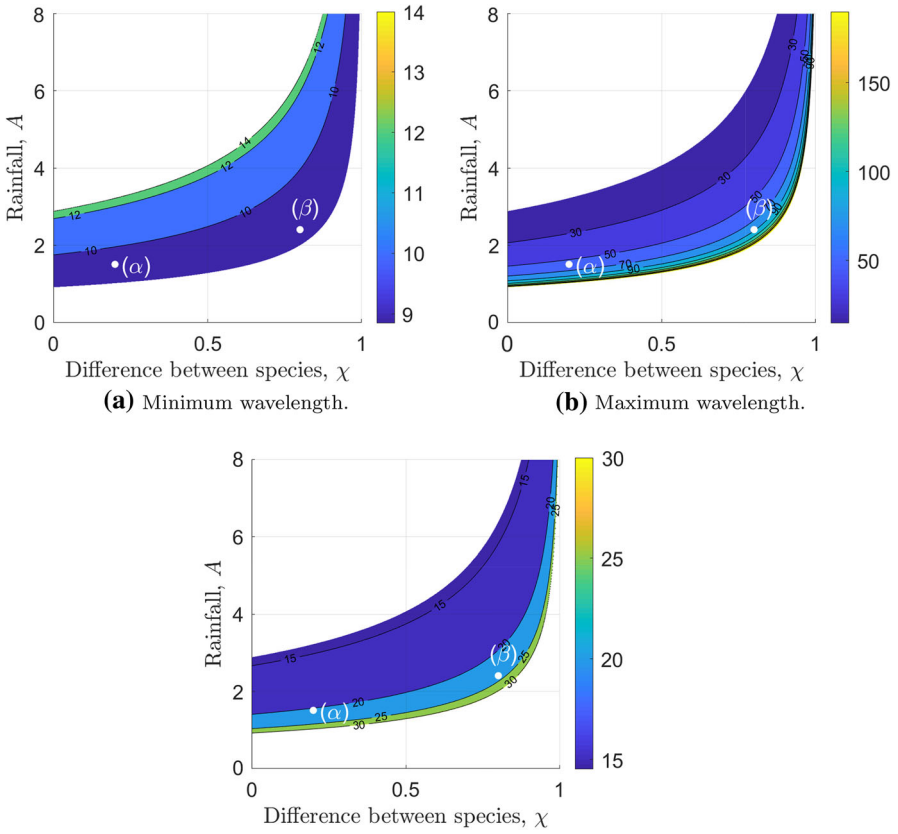

(a) Minimum wavelength.

(b) Maximum wavelength.

(c) Wavelength arising from most unstable wavenumber.

Fig. 3 Single species pattern wavelength. This figure visualises the pattern wavelengths of both single-species patterns calculated through linear stability analysis. The contours show the wavelength of the pattern of species u_2 as its difference from the grass species u_1 increases, while the values on the A-axis correspond to the wavelength of the grass pattern. Minimum (**a**), maximum (**b**) and wavelengths corresponding to the most unstable mode (**c**) are shown. The parameter values are $B_1 = 0.45, b_2 = 0.0055$, $f = 0.01, h = 0.01$, $D_0 = 0.01$ and $d = 500$. The markers (α) and (β) refer to the parameter values used in the simulations presented in Fig. 1. For a comparison to the wavelengths of the coexistence pattern, see Fig. 7 (Color figure online)

under suitable conditions that ensure their existence and biological relevance. For $(\overline{u}_1^{C,-}, \overline{u}_2^C, \overline{w}^{C,-})$ these are $B_2 > B_1 F$ and

$$\max\left\{\frac{B_2\left(\overline{u}_2^C\,(1-H)+2\right)}{F}, \frac{B_2\overline{u}_2^C\,(1+F)}{F}\right\} < A < \frac{B_2\left(1+H\left(\overline{u}_2^C\right)^2\right)}{FH\overline{u}_2^C},$$

while the corresponding conditions for $(\overline{u}_1^{C,+}, \overline{u}_2^C, \overline{w}^{C,+})$ are $B_2 > B_1 F$ and

$$A > A_{\min}^{C,+} := \max\left\{\frac{B_2\left(\overline{u}_2^C(1-H)+2\right)}{F}, \min\left\{\frac{B_2\overline{u}_2^C(1+F)}{F}, \frac{B_2\left(1+H\left(\overline{u}_2^C\right)^2\right)}{FH\overline{u}_2^C}\right\}\right\}. \tag{15}$$

Visualisations in this paper are shown for the special parameter setting (5) and $F = H$. In this situation changes to χ do not affect the nature of how the equilibrium loses its relevance. If $s > b_2 - B_1 f$, then $(\overline{u}_1^{C,+}, \overline{u}_2^C, \overline{w}^{C,+})$ ceases to exist at $A = A_{\min}^{C,+}$, while otherwise $A = A_{\min}^{C,+}$ represents the threshold at which $\overline{u}_1^{C,+}$ becomes negative (see Fig. 4). Similar considerations hold for $(\overline{u}_1^{C,-}, \overline{u}_2^C, \overline{w}^{C,-})$. This equilibrium, however, does not exhibit the metastability property which is the main focus of this paper and is therefore not considered further. It is noteworthy that there is nothing special about the choice of $F = H$ and results are robust to changes in F and H, provided the rainfall minimum $A_{\min}^{C,+}$ remains in the biologically relevant parameter region. Results presented in this paper are also robust to changes in s. Finally, we remark that the size of the shading parameter S needs to be similar to that of the average fitness difference between both species $B_2 - B_1 F$ for the equilibrium to remain in a biologically relevant region, as large (small) shading effects only support coexistence at equilibrium if the density of u_2 is low (high).

An initial conclusion that is drawn from calculation of the existence region of the coexistence equilibria is that their existence is not required for metastable patterns in which both species coexist to form and patterns outside the existence region of $(\overline{u}_1^{C,\pm}, \overline{u}_2^C, \overline{w}^{C,\pm})$ truly originate from a stable tree-only pattern as discussed in Sect. 4. In particular, the simulation shown in Fig. 1b is obtained by using parameter values for which the coexistence steady states do not exist (see the (β) marker in Fig. 4a). The parameter region considered in this section may, however, overlap with that considered in Sect. 4, and no general statement on the sizes of $A_{\min}^T$ and $A_{\min}^{C,+}$ can be made.

To gain a better understanding of the effects caused by the difference in both plant types, it is essential to understand the steady states' behaviour if the species are identical. At $\chi = 0$, the coexistence steady state is

$$\left(\overline{u}_1^{C,\pm}, \overline{u}_2^C, \overline{w}^{C,\pm}\right) = \left(\frac{\left(A \pm \sqrt{A^2 - 4B_1^2}\right)}{2B_1} - \frac{b_2 - B_1 f}{s}, \frac{b_2 - B_1 f}{s}, \frac{2B_1^2}{A \pm \sqrt{A^2 - 4B_1^2}}\right). \tag{16}$$

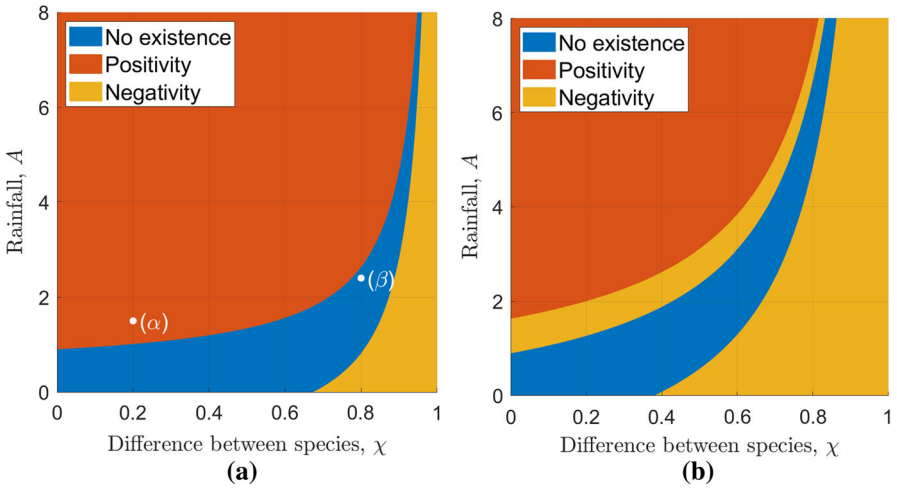

Fig. 4 Existence and positivity of the coexistence steady state. Visualisation of the parameter regions in which the coexistence steady state $(\overline{u}_1^{C,+}, \overline{u}_2^C, \overline{w}^{C,+})$ exists and is biologically relevant (positive) in the χ-A parameter plane for different levels of shading. In (**a**) $s = 10^{-3}$, while in (**b**) $s = 3 \cdot 10^{-4}$. The other parameter values used in this visualisation are $B_1 = 0.45$, $b_2 = 0.0055$, $f = 0.01$ and $h = 0.01$. The legend of (**a**) also applies to (**b**). The markers (α) and (β) in (**a**) refer to the parameter values used in the simulations presented in Fig. 1 (Color figure online)

As remarked in Sect. 2, for $\chi = 0$, the densities $u_1 + u_2$ and w satisfy the extended Klausmeier model. Thus, the sum $u_1 + u_2$ gives rise to a continuum of steady states that satisfy

$$u_1 + u_2 = \frac{A \pm \sqrt{A^2 - 4B_1^2}}{2B_1^2}, \quad \text{and} \quad w = \frac{2B_1^2}{A \pm \sqrt{A^2 - 4B_1^2}}.$$

The coexistence steady state $(\overline{u}_1^{C,\pm}, \overline{u}_2^C, \overline{w}^{C,\pm})$ maps to one member of this continuum whose choice depends on the model parameters as given by (16).

5.1 Stability to Spatially Uniform Perturbations

Similar to the analysis in Sect. 4, linear stability analysis can be used to investigate the existence of patterns arising from the coexistence steady state $(\overline{u}_1^{C,\pm}, \overline{u}_2^C, \overline{w}^{C,\pm})$. The algebraic complexity of the Jacobian with entries (7) evaluated at both coexistence equilibria does not allow an analytic derivation of stability conditions similar to those for the single-species states in Sect. 4. Instead, we performed a systematic numerical investigation of the Jacobian's eigenvalues $\lambda_u^{C,\pm} \in \mathbb{C}$ that determine the steady states' stability to spatially uniform perturbations in the respective positivity regions. This suggests that both steady states are unstable. The instability of $(\overline{u}_1^{C,+}, \overline{u}_2^C, \overline{w}^{C,+})$, however, is caused by an eigenvalue of small size, denoted by $\lambda_{u,1}^{C,+}$,

i.e. $0 < \max_{\lambda_u}\{Re(\lambda_u^{C,+})\} = Re(\lambda_{u,1}^{C,+}) \ll 1$, where the maximum is taken over all eigenvalues $\lambda_u^{C,+}$ of the Jacobian $J^{C,+} = (j)_{k\ell}^{C,+}, k, \ell = 1, 2, 3$ evaluated at the steady state (see Fig. 5a). The metastability associated with the small size of $Re(\lambda_{u,1}^{C,+})$ is, as in the case discussed in Sect. 4, due to the species' similar average fitness, i.e. the small difference of $B_2 - B_1 F$. Indeed, an application of determinant-preserving elementary row operations shows

$$\begin{aligned}\det\left(J^{C,+}\right) &= \det\begin{pmatrix} j_{11}^{C,+} & j_{12}^{C,+} & j_{13}^{C,+} \\ 0 & B_2 - B_1 F & 0 \\ j_{31}^{C,+} & j_{32}^{C,+} & j_{33}^{C,+} \end{pmatrix} \\ &= (B_2 - B_1 F)\left(j_{11}^{C,+} j_{33}^{C,+} - j_{13}^{C,+} j_{31}^{C,+}\right) = O\left(B_2 - B_1 F\right).\end{aligned}$$

The equilibrium is only of biological relevance if $B_2 > B_1 F$. Thus, as discussed in Sect. 4.2, $|B_2 - B_1 F| \ll 1$, and hence $|\det J| \ll 1$. Since the determinant of a matrix is the product of its eigenvalues, this shows the small size of one of the Jacobian's eigenvalues. If $B_2 - B_1 F = 0$ but $S \neq 0$, then the coexistence steady state $(\overline{u}_1^{C,\pm}, \overline{u}_2^{C}, \overline{w}^{C,\pm})$ reduces to the grass-only equilibrium $(\overline{u}_1^{G,\pm}, 0, \overline{w}^{G,\pm})$ and the small eigenvalue $\lambda_{u,1}^{C,+}$ of the coexistence state corresponds to $\lambda_{u,1}^{G,\pm}$ which vanishes because $B_2 - B_1 F = 0$.

5.1.1 Metastable States

For a system initially close to the coexistence steady state $(\overline{u}_1^{C,+}, \overline{u}_2^{C}, \overline{w}^{C,+})$, the small size of the only positive real part of the Jacobian's eigenvalues leads to a slow transition away from the equilibrium in the spatially uniform setting. If spatially non-uniform perturbations of the steady state are considered, this transition occurs via metastable coexistence patterns of both species, subject to sufficiently low rainfall levels. This is quantified by linear stability analysis which shows that the maximum real part of the corresponding Jacobian's eigenvalues exceeds $Re(\lambda_{u,1}^{C,+})$ by several orders of magnitude (see Fig. 5b, c for a visualisation). In other words, $\max_{k\geq 0}\{Re(\lambda_{s,1}^{C,+}(k^2))\} \gg Re(\lambda_{u,1}^{C,+})$, where $\lambda_{s,1}^{C,+}(k^2)$ denotes the eigenvalue of $J^{C,+} - \mathrm{diag}(k^2, Dk^2, dk^2)$ with the largest real part. This leads to a quick establishment of a coexistence pattern about the steady state from a spatially non-uniform perturbation which then persists for a long time before transiting to a stable one-species state. The growth rate that causes the formation of spatial patterns is given by

$$Re\left(\lambda_{s,1}^{C,+}\left(k^2\right)\right) = \alpha\left(k^2\right) + Re\left(\frac{\left(\beta\left(k^2\right) + \sqrt{\gamma\left(k^2\right)}\right)^{\frac{2}{3}} + \delta\left(k^2\right)}{\left(\beta\left(k^2\right) + \sqrt{\gamma\left(k^2\right)}\right)^{\frac{1}{3}}}\right), \tag{17}$$

where α, β, γ and δ are polynomials in k^2. Due to the algebraic complexity of the eigenvalue, an analytic determination of the pattern-defining features is impractical.

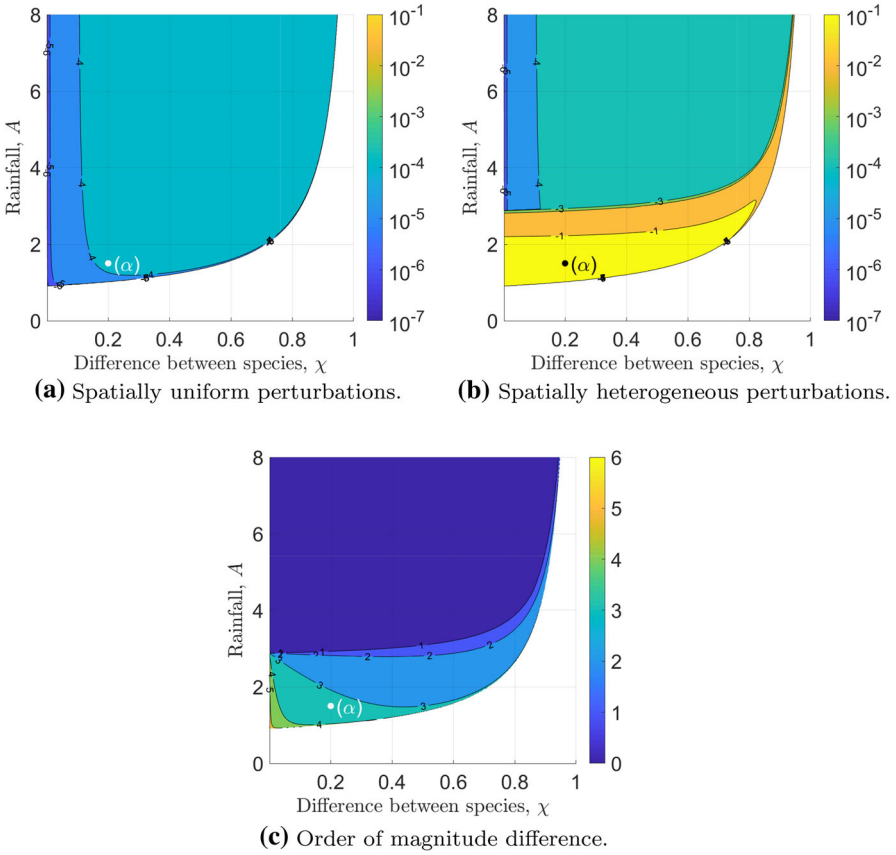

(a) Spatially uniform perturbations. **(b)** Spatially heterogeneous perturbations.

(c) Order of magnitude difference.

Fig. 5 Largest real part of eigenvalues determining stability of the coexistence steady state. Visualisation of $\max_{k>0}\{Re(\lambda^{C,+}_{\cdot,1})\}$ in the χ-A parameter plane for the coexistence equilibrium $(\overline{u}^{C,+}_1, \overline{u}^{C}_2, \overline{w}^{C,+})$, where $\lambda^{C,+}_{\cdot,1}$ denotes the eigenvalue with largest real part of the Jacobian with entries (7) evaluated at the steady state that determine its stability to spatially uniform (**a**) and spatially heterogeneous (**b**) perturbations. The order of magnitude difference between the results for spatially uniform and spatially heterogeneous perturbations is shown in (**c**). White areas indicate regions in which the steady state is negative or does not exist. The plots are obtained by evaluating $\max_{k>0}\{Re(\lambda^{C,+}_{\cdot,1})\}$ for $0 < A < 8$ and $0 < \chi < 1$ with increments $\Delta A = 0.01$ and $\Delta\chi = 0.001$. The parameters are $s = 10^{-3}$, $B_1 = 0.45$, $b_2 = 0.0055$, $f = 0.01$, $h = 0.01$, $D_0 = 0.01$, $d = 500$. The marker (α) refers to the parameter values used in the simulations presented in Fig. 1a (Color figure online)

Instead, we studied it numerically to determine the existence and possible wavelengths of a metastable pattern.

As rainfall A increases from the minimum $A^{C,+}_{\min}$, $\max_{k\geq 0}\{Re(\lambda^{C,+}_{s,1}(k^2))\}$ decreases and there exists a critical value of precipitation $A^{C,+}_{\max}$ beyond which $\max_{k\geq 0}\{Re(\lambda^{C,+}_{s,1}(A;k^2))\} = Re(\lambda^{C,+}_{u,1}(A))$ (Fig. 6a). In particular, there is a discontinuity in $k^{C,+}_{\max} := \arg\max_{k\geq 0}\{Re(\lambda^{C,+}_{s,1}(k^2))\}$ at $A = A^{C,+}_{\max}$, because the maximum real part of the eigenvalues attains its maximum at $k = 0$ for $A > A^{C,+}_{\max}$, but $k^{C,+}_{\max} \nrightarrow 0$

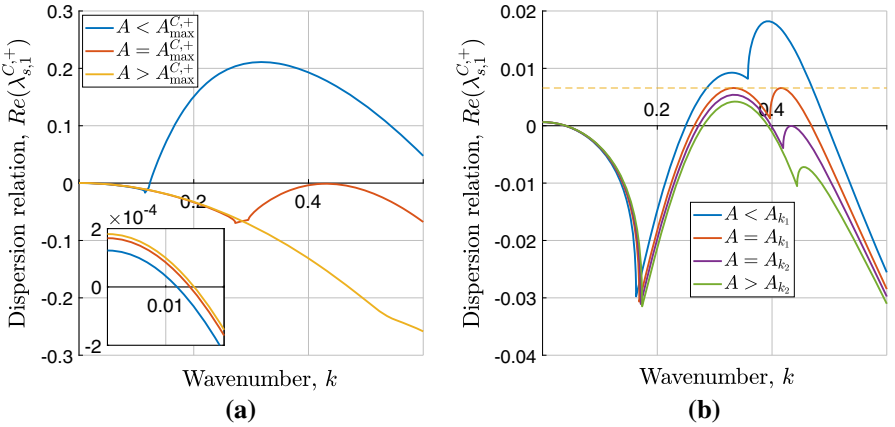

Fig. 6 Dispersion relation for patterns with species coexistence. The dispersion relation is visualised for different rainfall levels A and fixed $\chi = 0.2$ (**a**) and $\chi = 0.86$ (**b**). The inset in (**a**) shows the behaviour close to the origin. The dotted line in (**b**) indicates the equality of the local maxima for $A = A_{k_1}$. The other parameters are $s = 10^{-3}$, $B_1 = 0.45$, $b_2 = 0.0055$, $f = 0.01$, $h = 0.01$, $D_0 = 0.01$, $d = 500$ (Color figure online)

as $A \uparrow A_{\max}^{C,+}$. This threshold is an upper bound for the existence of metastable coexistence patterns and is visualised in Fig. 5c. For rainfall levels above this threshold, metastable coexistence of both plant species still occurs, albeit not as a pattern. Spatial heterogeneity does not cause the formation of patterns in this case as $Re(\lambda_{s,1}^{C,+}(A))$ attains its maximum at $k = 0$. The small size of $Re(\lambda_{u,1}^{C,+})$ still causes a solution slightly perturbed from the coexistence steady state to remain close to the equilibrium for a long time. This gives rise to a metastable state in which both vegetation types are present uniformly in space.

5.1.2 Wavelength

Linear stability analysis further provides an insight into the wavelength of patterns. Typically the wavelength of a pattern is dominated by the wavenumber yielding the largest growth. However, since the wavelength of a pattern is an inherently nonlinear property different modes may be selected due to effects such as hysteresis. In this case the roots of $Re(\lambda_{s,1}^{C,+}(k^2))$ provide an upper and lower bound for the wavelength. The numerical investigation of the dispersion relation shows that pattern wavelength increases with decreasing rainfall, in line with results shown in Sect. 4 and previous results on the single-species Klausmeier model on sloped ground (Sherratt 2005, 2013c). In other words, the distance between vegetation patches is larger in regions in which a smaller amount of the limiting water resource is available. An increase in the difference between the two plant species also causes an increase in the wavelength difference, but this increase is small compared to changes caused by precipitation fluctuations. A visualisation of the wavelength is given in Fig. 7. A further complication in the calculation of the wavelength through linear stability analysis arises through the algebraic complexity of the dispersion relation (17) which causes a discontinuity

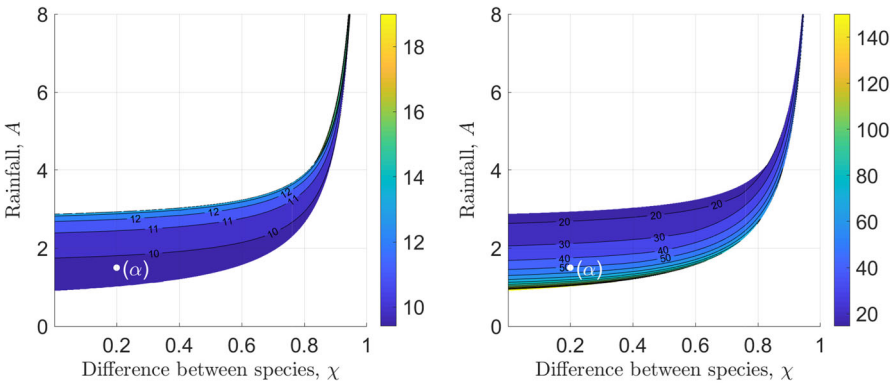

(a) Minimum wavelength. **(b)** Maximum wavelength.

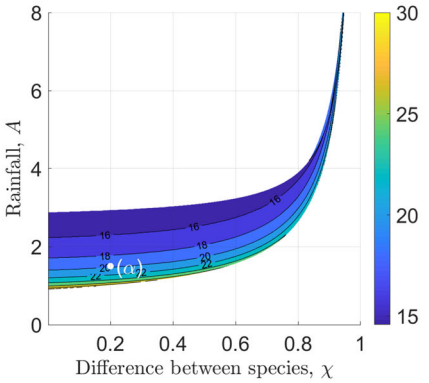

(c) Wavelength arising from most unstable wavenumber.

Fig. 7 Wavelength of metastable coexistence patterns. This figure visualises contours of the wavelength associated with the wavenumber yielding the largest growth (**c**) as well as lower (**a**) and upper bounds (**b**) that arise from linear stability analysis. For details on the creation of the plots and the parameter values, see Fig. 5. For a comparison to the wavelengths of the single-species pattern, see Fig. 3 (Color figure online)

in the most unstable mode and hence also the largest root in a subset of the parameter space considered in this analysis. The discontinuities arise from the existence of two local maxima of $Re(\lambda_{s,1}^{C,+}(k^2))$, one of which occurs for $k_1 < k < k_2$, which is the positivity region of $\gamma(k^2)$, while the other local maximum is attained for $k > k_2$. Consequently, there exists a critical value of the precipitation parameter A_{k_1} at which there is a discontinuity in $\arg\max_{k\geq 0} Re(\lambda_{s,1}^{C,+}(k^2))$ because both local maxima coincide (see Fig. 6b). Similarly, the rainfall value A_{k_2} at which $\max_{k\geq k_2} Re(\lambda_{s,1}^{C,+}(k^2)) = 0$, causes a discontinuity in the largest root of the dispersion relation and thus in the lower bound for the wavelength of the coexistence pattern.

6 Discussion

Our work predicts that coexistence of two plant species competing for the same limiting resource can occur as a long transient state, even if coexistence is inherently unstable. Such a metastable behaviour is characterised by the small size of the only positive eigenvalue of the equilibrium from which the coexistence arises. Coexistence of two species in such a metastable state is enabled by a balance of both species' average fitness which is measured by the ratio of a species' capability to convert water into new biomass to its mortality rate. In the nondimensional model parameters, this balance corresponds to the small size of $B_2 - B_1 F$, the quantity that controls the size of the eigenvalue causing the instability.

In ecology, the understanding of transient states is of utmost importance as many ecosystems never reach an equilibrium state. Disturbances such as changes to grazing patterns or climate change interrupt the convergence to a steady state on a frequent basis, and thus keep systems in perpetual transients (Sprugel 1991; Svenning and Sandel 2013). The occurrence of such disequilibrium states is not specific to savanna and dryland biomes but also occurs in ecosystems of other climate zones (Serra-Diaz et al. 2018). While we have not investigated the system's response to changes in environmental conditions, such as variability in precipitation or a changes in water evaporation due to temperature fluctuations, the analysis presented in this paper can provide an insight into the dynamics of such transient states by investigating their origin, fate and some of their properties.

We have established two possible origins of metastable states in the multispecies model (4): a spatially uniform equilibrium in which both species coexist (Sect. 5) and a one-species tree pattern that is unstable to the introduction of the herbaceous species (Sect. 4). For the latter, the consideration of the interspecific shading feedback is not necessary. The direct interspecific competition does, however, cause a further decrease in the unstable eigenvalue (14), by further reducing the average fitness difference between both species. Large shading effects may also tip that balance in favour of the tree species, stabilising the tree pattern and thus preventing the formation of a metastable coexistence pattern from an invasion-type scenario (see Fig. 2).

On the other hand, the inclusion of the shading effect is essential for the existence of metastable states arising from a coexistence equilibrium as a direct interspecific competition term is necessary for the existence of such a steady state. Coexistence at equilibrium without the presence of a shading effect is only possible if the average fitness of both species are equal, i.e. $B_2 = B_1 F$, a highly unlikely scenario unless both species are the same. Similar to a previous analysis of a multispecies model in dryland ecosystems by Nathan et al. (2013), we did not consider this special case as it lacks biological relevance. Nevertheless, the lack of a shading feedback does not necessarily prevent the establishment of a coexistence pattern from perturbations to a spatially uniform configuration of both species similar to that visualised in Fig. 1a. If the species differ in their dispersal behaviour, the faster dispersing species can establish a spatial pattern (provided precipitation is sufficiently low) and can act as an ecosystem engineer by redistributing the water resource to which the slow disperser can adapt and form a pattern itself. As discussed in slightly different settings by Nathan et al. (2013) and Baudena and Rietkerk (2013), this supports the existence of coexistence

patterns. In particular, this pushes the system into a state to which the theory presented in Sect. 4 can be applied. Hence, if one of the two corresponding single-species states is unstable to the introduction of the competitor via a very small eigenvalue, the system remains in the coexistence pattern state for a long time. This observation emphasises the difficulty of inferring the origin of a metastable multispecies patterned state, which is beyond the scope of this paper.

The wavelength of the pattern may provide a useful tool in predicting the fate of a coexistence pattern, but potential shortfalls (linearisation, neglection of hysteresis effects) in the determination of the wavelength need to be taken into account. Our analysis of the patterns' wavelengths shows that the wavelength of a single-species tree pattern (Fig. 3) is very similar to that of a pattern in which the tree species coexists with the grass species (Fig. 7). However, if both species differ significantly (the parameter χ being close to unity), linear stability analysis predicts single-species grass patterns at a smaller wavelength than coexistence patterns. Thus, if a pattern in which both species coexist occurs at an atypical mode that differs from the results presented in Sects. 4.2.1 and 5.1.2 and better fits the wavelength prediction of a one-species pattern (such as in the later stages of the solution visualised in Fig. 1b), it can be concluded that the metastable pattern eventually reduces to a one-species pattern to which the observed wavelength corresponds.

We have restricted our analysis in this paper to the two-species model (4) to focus on the analytical investigation of pattern existence. Numerical simulations of a three-species model similar to (2) with $n = 3$, but with the addition of multiple, hierarchical interspecific interaction terms, also yield metastable patterned solutions in which all three species coexist, provided their average fitness differences are small. Coexistence through metastability can further occur for just a subset of all species in the model. Indeed, our numerical experiments show that if one of the species has a lower average fitness, then the community of superior species outcompetes the inferior species on a short timescale and forms a metastable coexistence state in which it remains on a long timescale. We thus hypothesise that the metastability property discussed in this paper is not specific to the two-species model (4) but can be extended to a larger community of plant species in desert ecosystems. Moreover, our simulations of the three-species model indicate that the crucial condition for the existence of metastable solutions–small average fitness differences between species—is carried over to systems of more diverse plant communities.

The concept of a metastable solution to a system is not new. Metastability has, for example, been studied in the Cahn–Hilliard equation (Bates and Xun 1994, 1995), in chemotactic models (Potapov and Hillen 2005) and microwave heating models (Iron and Ward 2004). The occurrence of a slow transient between two stable states has even been briefly commented on in the analysis of a more complex multispecies model of desert plants (Gilad et al. 2007b), without the attempt to provide a detailed investigation of the phenomenon. It is worth emphasising that we characterise metastability by the small size of the only positive eigenvalue of an equilibrium. In landscape ecology, however, the term metastability usually has a broader meaning as it describes a stable system whose single components are changing over time due to disturbance and recovery effects (Zimmerman et al. 2010).

The model in this paper is based on the Klausmeier model (Klausmeier 1999), which deliberately reduces the description of the dynamics responsible for the formation of vegetation patterns in arid environments to the infiltration feedback arising from a soil modification caused by plants. A range of more complex models exist (see Zelnik et al. (2013) for a review of the most commonly used models) that capture a number of additional features of dryland ecosystems, such as nonlocal plant dispersal (Alfaro et al. 2018; Baudena and Rietkerk 2013; Eigentler and Sherratt 2018; Pueyo et al. 2008, 2010), different dynamics of soil and surface water (HilleRisLambers et al. 2001; Rietkerk et al. 2002), nonlocal water uptake due to extended root networks (Gilad et al. 2004), more realistic grazing/browsing effects (Siero 2018; Siero et al. 2019) or autotoxicity (Marasco et al. 2014). Simulation-based approaches have to some extent addressed the influence of these feedbacks on the coexistence of species (Gilad et al. 2007b; Kyriazopoulos et al. 2014), but an analytical approach similar to that presented in this paper may provide further insight into the way in which these additional assumptions affect coexistence mechanisms.

A natural extension of the work presented in this paper would be an investigation of the metastability property in a two-dimensional space domain. The linear stability analysis from Sects. 4 and 5 can be carried over to a higher space dimension, but does not provide any new information on the metastable behaviour of a patterned solution. Instead, numerical simulations could provide more insights into the coexistence pattern's properties away from the Turing bifurcation locus, such as a classification of its type (gap pattern, labyrinth pattern, stripe pattern or spot pattern) along the precipitation gradient (Meron 2012). The combination of adding an additional space dimension with the long runtimes required to capture the metastable behaviour of the system would, however, incur a significant computational cost.

A final area of potential future work concerns variabilities in environmental conditions, which have not been addressed in this paper. Effects such as rainfall seasonality (Baudena et al. 2007; Guttal and Jayaprakash 2007; Kletter et al. 2009), rainfall intermittency (Baudena et al. 2007; Kletter et al. 2009; Siteur et al. 2014b; Ursino and Contarini 2006), periodic variation in precipitation (Tzuk et al. 2019) or topographic heterogeneity (Gandhi et al. 2018) are known to be significant for vegetation patterns and have been studied using single-species models. It could therefore be of interest to extend those approaches to multispecies ecosystems to develop an understanding of how such heterogeneities affect the coexistence of species and, in particular, the metastability property of the model presented in this paper. Indeed, simulations of our multispecies model under seasonal precipitation regimes suggest that rainfall seasons of intermediate length (150–250 days per year) prolong the time the system remains in a coexistence state. Initial simulations, however, also suggest that inherently nonlinear properties such as pattern wavelength have a significant effect on the system's transient behaviour under temporal variations of environmental conditions. A detailed investigation of this phenomenon is therefore beyond the scope of this paper, but would present new valuable insights into coexistence of plant species in dryland ecosystems.

References

Alfaro M, Izuhara H, Mimura M (2018) On a nonlocal system for vegetation in drylands. J Math Biol 77:1761–1793

Bastiaansen R, Jaïbi O, Deblauwe V, Eppinga MB, Siteur K, Siero E, Mermoz S, Bouvet A, Doelman A, Rietkerk M (2018) Multistability of model and real dryland ecosystems through spatial self-organization. In: Proceedings of the National Academy of Sciences, pp 201804771

Bates P, Xun J (1994) Metastable patterns for the Cahn–Hilliard equation, part I. J Differ Equ 111:421–457

Bates P, Xun J (1995) Metastable patterns for the Cahn–Hilliard equation: part II. Layer dynamics and slow invariant manifold. J Differ Equ 117:165–216

Baudena M, Rietkerk M (2013) Complexity and coexistence in a simple spatial model for arid savanna ecosystems. Theor Ecol 6:131–141

Baudena M, Boni G, Ferraris L, von Hardenberg J, Provenzale A (2007) Vegetation response to rainfall intermittency in drylands: results from a simple ecohydrological box model. Adv Water Resour 30:1320–1328

Baudena M, D'Andrea F, Provenzale A (2010) An idealized model for tree–grass coexistence in savannas: the role of life stage structure and fire disturbances. J Ecol 98:74–80

Bennett JJ, Sherratt JA (2018) Long-distance seed dispersal affects the resilience of banded vegetation patterns in semi-deserts. J Theor Biol. https://doi.org/10.1016/j.jtbi.2018.10.002

Borgogno F, D'Odorico P, Laio F, Ridolfi L (2009) Mathematical models of vegetation pattern formation in ecohydrology. Rev Geophys 47:RG1005

Buis E, Veldkamp A, Boeken B, van Breemen N (2009) Controls on plant functional surface cover types along a precipitation gradient in the Negev Desert of Israel. J Arid Environ 73:82–90

Callegaro C, Ursino N (2018) Connectivity of niches of adaptation affects vegetation structure and density in self-organized (dis-connected) vegetation patterns. Land Degrad Dev 29:2589–2594

Consolo G, Currò C, Valenti G (2019) Supercritical and subcritical Turing pattern formation in a hyperbolic vegetation model for flat arid environments. Phys D Nonlinear Phenom. https://doi.org/10.1016/j.physd.2019.03.006

Cornet A, Delhoume J, Montaña C (1988) Diversity and pattern in plant communities. In: During H, Werger M, Willems H (eds) Dynamics of striped vegetation patterns and water balance in the Chihuahuan Desert. SPB Academic Publishing, The Hague, pp 221–231

Corrado R, Cherubini AM, Pennetta C (2014) Early warning signals of desertification transitions in semiarid ecosystems. Phys Rev E Stat Nonlinear Soft Matter Phys 90:062705

Dakos V, Kéfi S, Rietkerk M, van Nes EH, Scheffer M (2011) Slowing down in spatially patterned ecosystems at the brink of collapse. Am Nat 177:E153–E166

Deblauwe V, Barbier N, Couteron P, Lejeune O, Bogaert J (2008) The global biogeography of semi-arid periodic vegetation patterns. Glob Ecol Biogeogr 17:715–723

Deblauwe V, Couteron P, Bogaert J, Barbier N (2012) Determinants and dynamics of banded vegetation pattern migration in arid climates. Ecol Monogr 82:3–21

d'Herbès J-M, Valentin C, Tongway DJ, Leprun J-C (2001) Banded vegetation patterns and related structures. In: Tongway DJ, Valentin C, Seghieri J (eds) Banded vegetation patterning in arid and semiarid environments: ecological processes and consequences for management. Springer, New York, pp 1–19

Dickovick JT (2014) Africa 2014–2015. World today (Stryker). Rowman & Littlefield Publishers, Lanham, p 374

D'Onofrio D, Baudena M, D'Andrea F, Rietkerk M, Provenzale A (2015) Treegrass competition for soil water in arid and semiarid savannas: the role of rainfall intermittency. Water Resour Res 51:169–181

Dunkerley D, Brown K (2002) Oblique vegetation banding in the Australian arid zone: implications for theories of pattern evolution and maintenance. J Arid Environ 51:163–181

Eigentler L, Sherratt JA (2018) Analysis of a model for banded vegetation patterns in semi-arid environments with nonlocal dispersal. J Math Biol 77:739–763

Eldridge D, Zaady E, Shachak M (2000) Infiltration through three contrasting biological soil crusts in patterned landscapes in the Negev, Israel. CATENA 40:323–336

Gandhi P, Werner L, Iams S, Gowda K, Silber M (2018) A topographic mechanism for arcing of dryland vegetation bands. J R Soc Interface 15:20180508

Gilad E, von Hardenberg J, Provenzale A, Shachak M, Meron E (2004) Ecosystem engineers: from pattern formation to habitat creation. Phys Rev Lett 93:098105

Gilad E, von Hardenberg J, Provenzale A, Shachak M, Meron E (2007a) A mathematical model of plants as ecosystem engineers. J Theor Biol 244:680–691
Gilad E, Shachak M, Meron E (2007b) Dynamics and spatial organization of plant communities in water-limited systems. Theor Popul Biol 72:214–230
Gowda K, Iams S, Silber M (2018) Signatures of human impact on selforganized vegetation in the Horn of Africa. Engl Sci Rep 8:1–8
Gowda K, Chen Y, Iams S, Silber M (2016) Assessing the robustness of spatial pattern sequences in a dryland vegetation model. Proc R Soc Lond A 472:20150893
Guttal V, Jayaprakash C (2007) Self-organization and productivity in semiarid ecosystems: implications of seasonality in rainfall. J Theor Biol 248:490–500
Hemming CF (1965) Vegetation arcs in Somaliland. J Ecol 53:57–67
HilleRisLambers R, Rietkerk M, van den Bosch F, Prins HHT, de Kroon H (2001) Vegetation pattern formation in semi-arid grazing systems. Ecology 82:50–61
Iron D, Ward MJ (2004) The stability and dynamics of hot-spot solutions to two one-dimensional microwave heating models. Anal Appl 02:21–70
Kealy BJ, Wollkind DJ (2012) A nonlinear stability analysis of vegetative turing pattern formation for an interaction–diffusion plant-surface water model system in an arid flat environment. Bull Math Biol 74:803–833
Kéfi S, Rietkerk M, Alados CL, Pueyo Y, Papanastasis V, ElAich A, de Ruiter P (2007) Spatial vegetation patterns and imminent desertification in Mediterranean arid ecosystems. Nature 449:213–217
Klausmeier CA (1999) Regular and irregular patterns in semiarid vegetation. Science 284:1826–1828
Kletter A, von Hardenberg J, Meron E, Provenzale A (2009) Patterned vegetation and rainfall intermittency. J Theor Biol 256:574–583
Kyriazopoulos P, Nathan J, Meron E (2014) Species coexistence by front pinning. Ecol Complex 20:271–281
Marasco A, Iuorio A, Carteni F, Bonanomi G, Tartakovsky DM, Mazzoleni S, Giannino F (2014) Vegetation pattern formation due to interactions between water availability and toxicity in plant–soil feedback. Bull Math Biol 76:2866–2883
Meron E (2012) Pattern-formation approach to modelling spatially extended ecosystems. Ecol Model 234:70–82
Meron E (2016) Pattern formation—a missing link in the study of ecosystem response to environmental changes. Math Biosci 271:1–18
Meron E (2018) From patterns to function in living systems: dryland ecosystems as a case study. Annu Rev Condens Matter Phys 9:79–103
Montaña C (1992) The colonization of bare areas in two-phase mosaics of an arid ecosystem. J Ecol 80:315–327
Montaña C, Lopez-Portillo J, Mauchamp A (1990) The response of two woody species to the conditions created by a shifting ecotone in an arid ecosystem. J Ecol 78:789–798
Moreno-de las Heras MM, Saco PM, Willgoose GR, Tongway DJ (2012) Variations in hydrological connectivity of Australian semiarid landscapes indicate abrupt changes in rainfall-use efficiency of vegetation. J Geophys Res G Biogeosci 117:G03009
Müller J (2013) Floristic and structural pattern and current distribution of tiger bush vegetation in Burkina Faso (West Africa), assessed by means of belt transects and spatial analysis. Appl Ecol Environ Res 11:153–171
Nathan J, von Hardenberg J, Meron E (2013) Spatial instabilities untie the exclusion-principle constraint on species coexistence. J Theor Biol 335:198–204
Pelletier JD, De Long SB, Orem CA, Becerra P, Compton K, Gressett K, Lyons-Baral J, McGuire LA, Molaro JL, Spinler JC (2012) How do vegetation bands form in dry lands? Insights from numerical modeling and field studies in southern Nevada, USA. J Geophys Res F Earth Surf 117:F04026
Penny GG, Daniels KE, Thompson SE (2013) Local properties of patterned vegetation: quantifying endogenous and exogenous effects. Philos Trans Soc R London Ser A 371:20120359
Potapov AB, Hillen T (2005) Metastability in chemotaxis models. J Dyn Differ Equ 17:293–330
Pueyo Y, Kéfi S, Alados CL, Rietkerk M (2008) Dispersal strategies and spatial organization of vegetation in arid ecosystems. Oikos 117:1522–1532
Pueyo Y, Kéfi S, Díaz-Sierra R, Alados C, Rietkerk M (2010) The role of reproductive plant traits and biotic interactions in the dynamics of semiarid plant communities. Theor Popul Biol 78:289–297
Reynolds JF, Smith DMS, Lambin EF, Turner BL, Mortimore M, Batterbury SPJ, Downing TE, Dowlatabadi H, Fernandez RJ, Herrick JE, Huber- Sannwald E, Jiang H, Leemans R, Lynam T, Maestre FT, Ayarza

M, Walker B (2007) Global desertification: building a science for dryland development. Science 316:847–851
Rietkerk M, van de Koppel J (2008) Regular pattern formation in real ecosystems. Trends Ecol Evol 23:169–175
Rietkerk M, Ketner P, Burger J, Hoorens B, Olff H (2000) Multiscale soil and vegetation patchiness along a gradient of herbivore impact in a semi-arid grazing system in West Africa. Plant Ecol 148:207–224
Rietkerk M, Boerlijst MC, van Langevelde F, HilleRisLambers R, van de Koppel J, Kumar L, Prins HHT, de Roos AM (2002) Self-organization of vegetation in arid ecosystems. Am Nat 160:524–530
Rietkerk M, Dekker SC, de Ruiter PC, van de Koppel J (2004) Self-organized patchiness and catastrophic shifts in ecosystems. Science 305:1926–1929
Rodriguez-Iturbe I, Porporato A, Ridolfi L, Isham V, Coxi DR (1999) Probabilistic modelling of water balance at a point: the role of climate, soil and vegetation. Proc R Soc Lond A 455:3789–3805
Saco PM, Moreno-de las Heras M, Keesstra S, Baartman J, Yetemen O, Rodriguez JF (2018) Vegetation and soil degradation in drylands: non linear feedbacks and early warning signals. Curr Opin Environ Sci Health 5:67–72
Salvucci GD (2001) Estimating the moisture dependence of root zone water loss using conditionally averaged precipitation. Water Resour Res 37:1357–1365
Scheiter S, Higgins S, Weissing AEFJ, Geber EMA (2007) Partitioning of root and shoot competition and the stability of savannas. Am Nat 170:587–601
Seghieri J, Galle S, Rajot J, Ehrmann M (1997) Relationships between soil moisture and growth of herbaceous plants in a natural vegetation mosaic in Niger. J Arid Environ 36:87–102
Serra-Diaz JM, Maxwell C, Lucash MS, Scheller RM, Laflower DM, Miller AD, Tepley AJ, Epstein HE, Anderson-Teixeira KJ, Thompson JR (2018) Disequilibrium of fire-prone forests sets the stage for a rapid decline in conifer dominance during the twenty-first century. Sci Rep 8:6749
Sheffer E, Hardenberg J, Yizhaq H, Shachak M, Meron E, Blasius B (2013) Emerged or imposed: a theory on the role of physical templates and selforganisation for vegetation patchiness. Ecol Lett 16:127–139
Sherratt JA (2005) An analysis of vegetation stripe formation in semi-arid landscapes. J Math Biol 51:183–197
Sherratt JA (2010) Pattern solutions of the Klausmeier model for banded vegetation in semi-arid environments I. Nonlinearity 23:2657–2675
Sherratt JA (2011) Pattern solutions of the Klausmeier model for banded vegetation in semi-arid environments II: patterns with the largest possible propagation speeds. Proc R Soc Lond A 467:3272–3294
Sherratt JA (2013a) History-dependent patterns of whole ecosystems. Ecol Complex 14:8–20
Sherratt JA (2013b) Pattern solutions of the Klausmeier model for banded vegetation in semi-arid environments III: the transition between homoclinic solutions. Physica D 242:30–41
Sherratt JA (2013c) Pattern solutions of the Klausmeier model for banded vegetation in semiarid environments IV: slowly moving patterns and their stability. SIAM J Appl Math 73:330–350
Sherratt JA (2013d) Pattern solutions of the Klausmeier model for banded vegetation in semiarid environments V: the transition from patterns to desert. SIAM J Appl Math 73:1347–1367
Sherratt JA, Lord GJ (2007) Nonlinear dynamics and pattern bifurcations in a model for vegetation stripes in semi-arid environments. Theor Popul Biol 71:1–11
Siero E (2018) Nonlocal grazing in patterned ecosystems. J Theor Biol 436:64–71
Siero E, Siteur K, Doelman A, van de Koppel J, Rietkerk M, Eppinga MB (2019) Grazing away the resilience of patterned ecosystems. Am Nat 193:472–480
Siteur K, Siero E, Eppinga MB, Rademacher JD, Doelman A, Rietkerk M (2014a) Beyond turing: the response of patterned ecosystems to environmental change. Ecol Complex 20:81–96
Siteur K, Eppinga MB, Karssenberg D, Baudena M, Bierkens MF, Rietkerk M (2014b) How will increases in rainfall intensity affect semiarid ecosystems? Water Resour Res 50:5980–6001
Sprugel DG (1991) Disturbance, equilibrium, and environmental variability: What is 'natural' vegetation in a changing environment? Biol Conserv 58:1–18
Svenning J-C, Sandel B (2013) Disequilibrium vegetation dynamics under future climate change. Am J Bot 100:1266–1286
Synodinos AD, Tietjen B, Jeltsch F (2015) Facilitation in drylands: modeling a neglected driver of savanna dynamics. Ecol Model 304:11–21
Thiery JM, D'Herbès J-M, Valentin C (1995) A model simulating the genesis of banded vegetation patterns in Niger. J Ecol 83:497–507

Thompson SE, Harman CJ, Heine P, Katul GG (2010) Vegetation-infiltration relationships across climatic and soil type gradients. J Geophys Res G Biogeosci 115:G02023
Tilman D (1982) Resource competition and community structure. Princeton University Press, Princeton, p 296
Tongway DJ, Ludwig JA (1990) Vegetation and soil patterning in semi-arid mulga lands of Eastern Australia. Aust J Ecol 15:23–34
Tzuk O, Ujjwal SR, Fernandez-Oto C, Seifan M, Meron E (2019) Interplay between exogenous and endogenous factors in seasonal vegetation oscillations. Sci Rep 9:354
United Nations Convention to Combat Desertification (2017) The global land outlook. Version first edition, Bonn, Germany
United Nations Food and Agriculture Organization (2005) Livestock sector briefs
Ursino N, Callegaro C (2016) Diversity without complementarity threatens vegetation patterns in arid lands. Ecohydrology 9:1187–1195
Ursino N, Contarini S (2006) Stability of banded vegetation patterns under seasonal rainfall and limited soil moisture storage capacity. Adv Water Resour 29:1556–1564
Valentin C, d'Herbès J, Poesen J (1999) Soil and water components of banded vegetation patterns. CATENA 37:1–24
van der Stelt S, Doelman A, Hek G, Rademacher JDM (2013) Rise and fall of periodic patterns for a generalized Klausmeier–Gray–Scott model. J Nonlinear Sci 23:39–95
White LP (1971) Vegetation stripes on sheet wash surfaces. J Ecol 59:615–622
Worrall GA (1959) The Butana grass patterns. J Soil Sci 10:34–53
Zelnik YR, Kinast S, Yizhaq H, Bel G, Meron E (2013) Regime shifts in models of dryland vegetation. Philos Trans R Soc Lond Ser A 371:20120358
Zelnik YR, Gandhi P, Knobloch E, Meron E (2018) Implications of tristability in pattern-forming ecosystems. Chaos Interdiscip J Nonlinear Sci 28:033609
Zimmerman JK, Comita LS, Thompson J, Uriarte M, Brokaw N (2010) Patch dynamics and community metastability of a subtropical forest: compound effects of natural disturbance and human land use. Landsc Ecol 25:1099–1111